


2017

# Interfacial healing and transport phenomena modeling of biopolymers

Karla Enid Lebron  
*Iowa State University*

Follow this and additional works at: <https://lib.dr.iastate.edu/etd>

 Part of the [Agriculture Commons](#), [Bioresource and Agricultural Engineering Commons](#), [Materials Science and Engineering Commons](#), and the [Mechanics of Materials Commons](#)

---

## Recommended Citation

Lebron, Karla Enid, "Interfacial healing and transport phenomena modeling of biopolymers" (2017). *Graduate Theses and Dissertations*. 16161.  
<https://lib.dr.iastate.edu/etd/16161>

This Thesis is brought to you for free and open access by the Iowa State University Capstones, Theses and Dissertations at Iowa State University Digital Repository. It has been accepted for inclusion in Graduate Theses and Dissertations by an authorized administrator of Iowa State University Digital Repository. For more information, please contact [digirep@iastate.edu](mailto:digirep@iastate.edu).

# **Interfacial healing and transport phenomena modeling of biopolymers**

by

**Karla Lebron**

A thesis submitted to the graduate faculty  
in partial fulfillment of the requirements for the degree of

**MASTER OF SCIENCE**

Major: Agricultural and Biosystems Engineering

Program of Study Committee:  
David Grewell, Major Professor  
D. Raj Raman  
Martin Thuo

The student author, whose presentation of the scholarship herein was approved by the program of study committee, is solely responsible for the content of this thesis. The Graduate College will ensure this thesis is globally accessible and will not permit alterations after a degree is conferred.

Iowa State University

Ames, Iowa

2017

Copyright © Karla Lebron, 2017. All rights reserved.

**DEDICATION**

This work is dedicated to my Puerto Rican family.

## TABLE OF CONTENTS

	Page
LIST OF TABLES.....	v
LIST OF FIGURES.....	vi
NOMENCLATURE.....	viii
ACKNOWLEDGEMENTS.....	ix
ABSTRACT.....	x
CHAPTER 1. INTRODUCTION AND OBJECTIVES .....	1
1.1 Introduction .....	1
1.2 Characteristics of Plastics.....	1
1.3 Welding of Plastics.....	6
1.4 Literature Review of Welding of PLA .....	7
1.5 Objectives.....	8
1.6 References .....	9
CHAPTER 2. WELDING OF PLA .....	10
2.1 Abstract .....	10
2.2 Introduction .....	10
2.3 Materials and Methods .....	13
2.3.1 Ingeo™ biopolymer 4032D .....	13
2.3.2 Ingeo™ biopolymer 2003D .....	13
2.3.3 Impulse welding for molecular healing measurements .....	13
2.3.4 Tensile testing .....	15
2.4 Results and Discussion.....	16
2.4.1 Impulse welding.....	16
2.5 Conclusion.....	19
2.6 References .....	20
CHAPTER 3. DEVELOPMENT OF MOLECULAR DIFFUSION MODELS FOR ULTRASONIC WELDING OF PLA .....	21
3.1 Abstract .....	21
3.2 Introduction .....	22
3.2.1 Ultrasonic welding .....	22
3.2.2 Molecular healing .....	23
3.3 Materials and Methods .....	31
3.3.1 Ingeo™ biopolymer 2003D .....	31
3.3.2 Ultrasonic welding for molecular healing validation.....	31

3.3.3 Tensile testing .....	35
3.3.4 FEA modeling with ANSYS.....	36
3.3.5 Heating model.....	39
3.4 Results and Discussion.....	39
3.4.1 Ultrasonic welding .....	39
3.4.2 Ultrasonic modeling.....	43
3.4.3 Model validation .....	50
3.5 Conclusion.....	55
3.6 References .....	56
CHAPTER 4. GENERAL CONCLUSIONS .....	57

## LIST OF TABLES

	Page
Table 2.1 Comparison of physical properties between PLA and commodity polymers.....	11
Table 3.1 Welding parameter used for molecular diffusion design of experiments for 21.6 $\mu\text{m}_{\text{p-p}}$ and 32.4 $\mu\text{m}_{\text{p-p}}$ amplitude.....	34
Table 3.2 Design of experiments for 21.6 $\mu\text{m}_{\text{p-p}}$ amplitude.....	40
Table 3.3 Design of experiments for 32.4 $\mu\text{m}_{\text{p-p}}$ amplitude.....	40
Table 3.4 Model theoretical power compared to measured machine power for both studied amplitudes.....	44
Table 3.5 Power (W) from ultrasonic welder at 21.6 $\mu\text{m}_{\text{p-p}}$ amplitude.....	46
Table 3.6 Power (W) from ultrasonic welder at 32.4 $\mu\text{m}_{\text{p-p}}$ amplitude.....	46
Table 3.7 Average heat flux (q) for 21.6 $\mu\text{m}_{\text{p-p}}$ .....	47
Table 3.8 Average heat flux (q) for 32.4 $\mu\text{m}_{\text{p-p}}$ .....	48

## LIST OF FIGURES

	Page
Figure 1.1 Details the lamellar fibril, crystalline and amorphous areas .....	4
Figure 1.2 Chemical structure of thermoplastic (amorphous and crystalline) and thermoset plastics .....	6
Figure 2.1 Impulse welder with heated elements on top and bottom fixtures .....	14
Figure 2.2 Time <sup>¼</sup> as a function of weld factor (Ingeo 2003D) .....	17
Figure 2.3 Temperature <sup>-1</sup> as a function of slope of weld factor (Ingeo 2003D) .....	18
Figure 2.4 Time <sup>¼</sup> as a function of weld factor (Ingeo 4032D) .....	18
Figure 2.5 Temperature <sup>-1</sup> as a function of slope of weld Factor (Ingeo 4032D) .....	19
Figure 3.1 Molecular diffusion and interfacial healing .....	23
Figure 3.2 Molecular diffusion and interfacial healing and Einstein's diffusion equation .....	24
Figure 3.3 Details impulse welding temperature profile .....	26
Figure 3.4 Details time increments in impulse welding temperature profile for degree of weld calculation .....	26
Figure 3.5 Plot of activation energy as a function for temperature for PS as report by Wool .....	27
Figure 3.6 Degree of healing as a function of time for polysulphone .....	28
Figure 3.7 Plot of natural log of slopes of as a function of inverse temperature (polysulphone) .....	29
Figure 3.8 Plot of ANSYS temperature profile for collapse distance of 0.1 mm, weld velocity of 0.1mm/s and amplitude of 21.6 µm p-p.....	30
Figure 3.9 PLA Rigid Sample (Ingeo 2003D).....	31
Figure 3.10 Dukane ultrasonic welder.....	32
Figure 3.11 Phases of the ultrasonic welding cycle.....	33
Figure 3.12 Phases of welding cycle as seen on iQ Explorer II software.....	34
Figure 3.13 Summary of molecular healing model development and verification.....	35
Figure 3.14 ANSYS volume (left), volume divided into elements through meshing function (center), and elements refined (right) .....	37
Figure 3.15 ANSYS thermal gradient without convection for collapse distance of 0.3 mm, weld velocity of 1mm/s and amplitude of 21.6 µm p-p (Sample C6) ...	38
Figure 3.16 ANSYS thermal gradient with convection for collapse distance of 0.3mm, weld velocity of 1mm/s and amplitude of 21.6 µm p-p (Sample C6) .....	38
Figure 3.17 Ultimate Stress as a function of collapse distance at 21.6 µm p-p amplitude.....	41
Figure 3.18 Ultimate Stress as a function of weld velocity at 21.6 µm p-p amplitude ....	42
Figure 3.19 Ultimate Stress as a function of collapse distance at 32.4 µm p-p amplitude	42
Figure 3.20 Ultimate Stress as a function of weld velocity at 32.4 µm p-p amplitude ....	43
Figure 3.21 Mathcad excerpt with material properties .....	44
Figure 3.22 Mathcad excerpt finding power (P) from volumetric heat rate (Q).....	46
Figure 3.23 Mathcad excerpt finding heat flux (q) from actual machine power (P) .....	47
Figure 3.24 ANSYS Temperature profile (°C as a function of time) .....	48
Figure 3.25 Type-K Thermocouple 36-gauge temperature profile.....	49

Figure 3.26 Excel excerpt of degree of weld calculation for 0.4 mm/s weld velocity, 0.1 mm weld distance and 21.6 $\mu\text{m}$ p-p amplitude (Sample A3) .....	49
Figure 3.27 Model validation at 21.6 $\mu\text{m}$ p-p amplitude and 0.1 mm collapse distance..	51
Figure 3.28 Model validation at 21.6 $\mu\text{m}$ p-p amplitude and 0.2 mm collapse distance..	51
Figure 3.29 Model validation at 21.6 $\mu\text{m}$ p-p amplitude and 0.3 mm collapse distance..	52
Figure 3.30 Collapsed data of actual weld strength as a function of predicted weld strength at 21.6 $\mu\text{m}$ p-p amplitude .....	52
Figure 3.31 Model validation at 32.4 $\mu\text{m}$ p-p amplitude and 0.1 mm collapse distance..	53
Figure 3.32 Model validation at 32.4 $\mu\text{m}$ p-p amplitude and 0.2 mm collapse distance..	54
Figure 3.33 Model validation at 32.4 $\mu\text{m}$ p-p amplitude and 0.3 mm collapse distance..	54
Figure 3.34 Collapsed data of actual weld strength as a function of predicted weld strength at 32.4 $\mu\text{m}$ p-p amplitude .....	55



**NOMENCLATURE**

$\theta$  Temperature ( $^{\circ}\text{C}$ )

$\lambda$  Thermal conductivity ( $\text{W}/(\text{m}\cdot^{\circ}\text{C})$ )

$\rho$  Density ( $\text{kg}/\text{m}^3$ )

$C$  Specific heat ( $\text{Joules}/(\text{kg}\cdot^{\circ}\text{C})$ )

$\varepsilon$  Mechanical Strain

$w_{\text{fay}}$  fay width

$K_0$  Diffusion material constant (J)

DW degree of healing (% or unitless)

$E_a$  Activation energy (J)

$E_{\text{loss}}$  Loss Modulus

$f$  Frequency (Hz)

$\omega$  Angular frequency (Rad/s)

$P$  Power (W)

$q$  Heat flux ( $\text{W}/\text{m}^2$ )

$Q$  Internal heat generation ( $\text{W}/\text{m}^3$ )

$R$  Boltzmann constant (J/K)

p-p Peak-to-peak

## ACKNOWLEDGEMENTS

I am profoundly grateful to have had an amazing group of mentors in this journey. Thank you to Dr. Grewell for the invaluable advice and guidance throughout this research process. I am thankful for the consistent dedication and support in all aspects during my time as his graduate student. I also want to thank Dr. D. Raj Raman and Dr. Martin Thuo for their advice, kind words and willingness to help provide the best feedback possible to me. Thank you also to my industry mentors in Dukane Corp. and Branson Ultrasonics Corp., especially to Leo Klinstein and Jeff Frantz, for providing their equipment for this research work as well as for their constant support and guidance. I also would like to thank the Center for Crop Utilization Research (CCUR), the National Science Foundation (NSF) and the Center for Bioplastics and Biocomposites (CB<sup>2</sup>) for the opportunity to be a part of this research and for providing financial support.

I would like to give special thanks to all my family. They have encouraged me throughout my entire journey and have been my greatest supporters from the very beginning. Thank you mom and dad for all your efforts and sacrifices to help me become who I am today. I do not take any of it for granted. This gratitude is extended to my sister Natasha. I could not ask for a better confidante. No matter the physical distance between us, your love and admiration gives me the strength to keep going.

I am also thankful for Iowa State and the friends and colleagues I have met along the way, especially Cindu, Mitch, Jake and Curtis for being a great support system. Finally, I cannot express enough gratitude to my best friend for his unwavering love and support. Ty'Jamin, thank you for always inspiring me and pushing me to be the best version of myself. Thank you for reminding me I can accomplish anything if I work hard enough.

**ABSTRACT**

This research focuses on the characterization of bioplastics joined using ultrasonic welding and modeling of temperature distributions and interfacial healing. Polylactic acid (PLA), which is typically derived from starch-rich crops such as corn, was studied. While the measurement of activation energy for interfacial healing at weld interfaces of PLA films has been reported, here, this information is used to predict the weld strength of rigid PLA samples welded by ultrasonics. A characterization of the mechanical properties was completed with a tensile test to determine the effects of amplitude, melt velocity and collapse distance on weld strength. From previous interfacial healing activation energy measurements based on an impulse welding method, it was also possible to predict weld strength.

It was found that the most influential parameters were weld time, collapse distance and weld velocity. In general, the model predicted weld strength reasonably well with  $r^2$  values between 0.77 and 0.78.

## CHAPTER 1

### INTRODUCTION AND OBJECTIVES

#### 1.1 Introduction

Thermoplastic materials have proven to have very useful applications in different industries such as the food, automotive, consumer products, and biomedical industry. Thermoplastics provide many advantages that stem from their intrinsic properties including low cost of manufacturing products as well relatively low material costs. This has allowed the plastics industry to grow to a volume larger than \$500B annually, whose products are mostly disposable in nature.

#### 1.2 Characteristics of plastics

Although polymers in general are often called plastics, there is an important difference. Polymers are extended macromolecular structures with many repeating units (poly) of molecules (mers). Synthetic plastics, DNA, cellulose from wood, and other natural products are all examples of polymers. However, the term plastics infers plasticity and the ability to be formed by a thermo-mechanical process. Not all polymers are plastic, *e.g.*, DNA and cellulose. When compared to natural polymers, such as cellulose, plastics tend to be less environmentally friendly because they often resist chemical break-down. In contrast, they do offer superior properties, such as high thermal stability. "Plastics" is the popular name for everyday plastic items such as "Styrofoam" cups and "Teflon" coatings and are generally man made. Elastomers are rubber-like polymers and general will return to their original shape after limited deformation. Even though polymers are not new, their advanced properties have opened many possibilities.

Natural rubber has been used for over three thousand years, but the use of natural rubber as the first raw material in the polymer age came with the discoveries by French explorers, Charles Marie de la Condamine (1701-1774) and Pierre Joseph Macquer (1718-1784) [1,2]. Natural rubber was first named as Caoutchouc. A paper published in 1763 by Macquer focused on purifying the substance and discovering a suitable solvent for rubber. This was the beginning of processing polymers and even today, novel polymers are still being developed [3].

The creation of synthetic rubber from isoprene using hydrochloric acid was first claimed by G. Bouchardat in 1879. Polystyrene was discovered accidentally by E. Simons in 1839 when cinnamic acid (gives fragrance in perfumes) was heated and allowed to sit for a few months. It was reported that a transparent, glass-like product with the same composition as styrene was produced [4,5]. In 1860, Marcellin Berthelot conducted extensive studies of the polymerization of styrene and was the first to identify substances as monomers or polymers using an empirical formula. The first Nobel Prize in chemistry was awarded for work that specifically included polymers conducted by Sir Walter Norman Haworth in 1937 for his work on polysaccharides.

With improved elemental analysis techniques available, the monomer unit of sugar and starch was identified as carbohydrate, with the empirical formula  $\text{CH}_2\text{O}$ . Furthermore, it was found that wood fiber and cellulose can be broken into monomers made of glucose. The polymerization of structurally different glucose yields polymers with different properties such as cellulose and starch, as explained by Haworth in 1927 [6].

The fully synthetic plastic era began with the production of first synthetic thermoset polymer, known as Bakelite (a phenol-formaldehyde), in 1907 by Leo Baekeland [7]. PVC was first produced in 1926 after a plasticizer (based on phthalate esters) was developed that

improved the flexibility of PVC. Plasticizers also helped to alleviate the rubber shortage at the beginning of World War II [8]. With the increase in industrial-scale polymer production, industry supported researches who were interested in developing useful structural or functional properties such as corrosion resistance, water resistance, lightweight, high fatigue resistance, and durability from polymers, and polymer composites have become the magic formula to success this reality. Charles Mackintosh (1766–1843) provided the very first example of composite plastics when he produced impregnated waterproof cloth by sandwiching a layer of rubber between two layers of cotton.

Thermal and mechanical properties of polymers and plastics are directly related to the morphological structure of the underlying macromolecular system. In thermoplastics, the two main structural states are the crystalline and the amorphous state. The structure of semi-crystalline polymers is comprised of varying crystalline and amorphous portions.

The perfect ordering of the macromolecular entities is called the crystalline state. This ordering can be in the form of stacks (lamella), shown in Figure 1.1, or in the folded form. An advantage of crystallinity is that it makes a material strong; however, excessive crystallinity can lead to brittleness. Many thermoplastic polymers will crystallize to some extent when the molten polymer is cooled to the melting point of the crystalline phase.

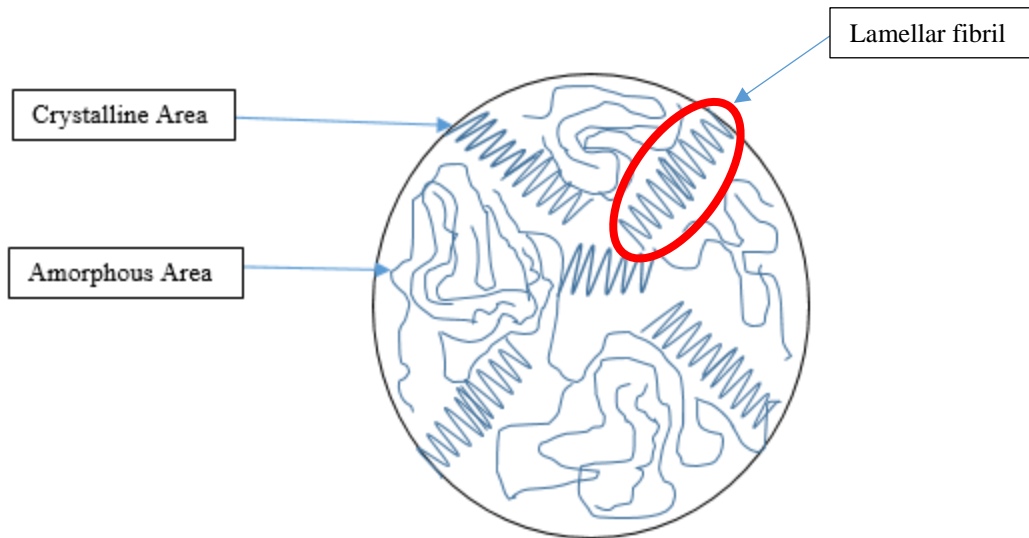


Figure 1.1. Details the lamellar fibril, crystalline and amorphous areas.

The degree of crystallinity depends on many parameters such as rate of cooling, the presence of orientation in the melt, melt temperature, and molar mass of the polymer. When polymer chains are disordered and entangled they are called amorphous polymers. Lacking crystallinity results in an amorphous polymer that has temperature dependent mechanical properties. Highly branched polymers or very low molecular weight polymer fractions contribute to the amorphous state; however, depending on parameters, such as cooling rates, other polymer structures can also promote amorphous structures. Polymer glasses and rubber are some common examples of amorphous polymers.

In general terms, plastics are divided into two main categories, thermoplastics and thermosets. Thermoplastic polymers are polymers that soften and harden reversibly when the temperature is changed. Both linear and branched polymers can act as thermoplastics. When thermoplastics are heated, they convert into a viscous liquid that is pliable or moldable. This property is very useful for fabrication processes, such as injection molding, extrusion molding, and blowing, where the thermoplastic polymers can be molded into complex shapes. Some

examples of thermoplastics are polyethylene, polypropylene, polystyrene, polycarbonate, and thermoplastic elastomers.

Thermoplastics are polymers with strong *intramolecular* but weak *intermolecular* interactions. These intermolecular interactions are sufficiently weak that, when heat or pressure is applied, the secondary bonds break and the polymer can flow. When the heat and pressure is removed, the reverse process occurs and the polymer typically returns to its “solid state”. Reversible intermolecular interactions in thermoplastics account for remolding/ reshaping capabilities in products.

Unlike thermoplastics, thermosetting polymers are made using partially polymerized precursors. With heat, or addition of a catalyst or radiation, these polymers crosslink and harden by curing undergoing non-reversible chemical reactions. Examples of thermosetting polymers are polyesters, epoxies, melamine, and silicone. Thermosetting polymers exhibit very strong intermolecular interactions because of their three-dimensional cross-linking or networking between polymeric molecules. The strong covalent bonds in the cross-links do not allow the reversible reaction upon increase in temperature. Therefore, these polymers do not soften in the presence of elevated temperature or pressure, but rather decompose once a critical temperature is reached, making thermosets ideal for high-heat applications. In addition to heat resistance, thermosets exhibit high levels of dimensional stability.

The main difference between these plastics is defined by their chemical structures; see Figure 1.2 [9].



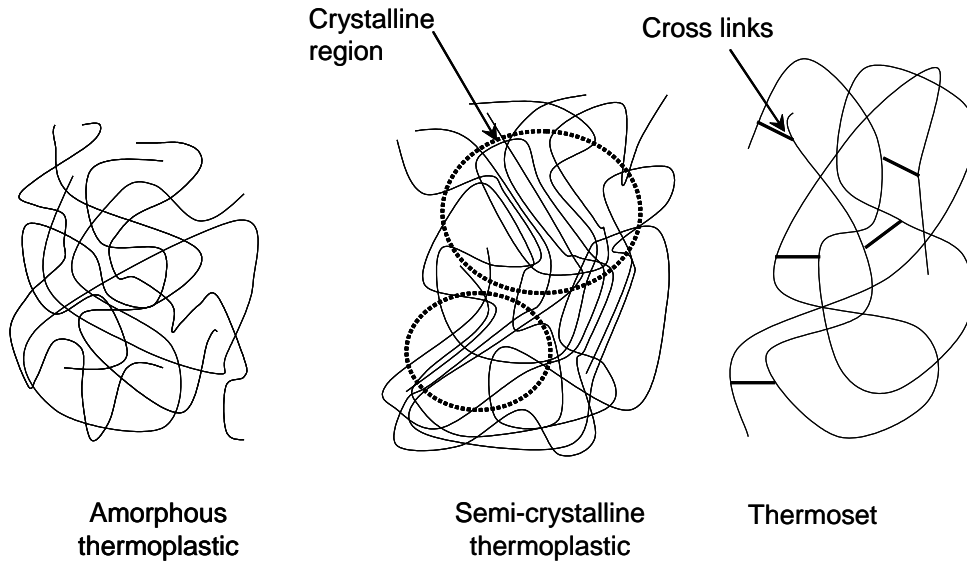


Figure 1.2. Chemical structure of thermoplastic (amorphous and crystalline) and thermoset plastics.

### 1.3 Welding of Plastics

In general, there are three techniques that can be used to join plastics:

- 1) Mechanical
- 2) Adhesives
- 3) Welding

While each of these processes has advantages and limitations, this thesis will focus on the welding technique.

A wide range of welding processes are used in industry to join plastics. Some of the most common techniques include:

- 1) Ultrasonic welding
- 2) Vibration welding
- 3) Heated tool welding
- 4) Laser welding
- 5) Radio frequency (RF/dielectric) welding

#### 6) Implant (resistance and induction) welding

It is beyond the scope of this thesis to detail these processes, but it is important to note that each process has advantages and limitations. This thesis will focus on ultrasonic and heated tool (impulse) welding.

### 1.4 Literature Review of Welding of PLA

Currently, all studies on ultrasonic welding and impulse welding of PLA cover only PLA films and investigated welding of rigid PLA parts. However, previous findings are valuable in examining which welding parameters are influential in determining weld quality. Stoehr N. *et al.* examined the influence of material composition on the processing window, that is, the range of welding parameters suitable to weld films efficiently and on weld quality [10].

Another study by J. Vogel describes the bonding of PLA “for a broad range of temperatures and contact times above the glass transition temperature in a lap shear joint geometry using an impulse welding system” [11]. This study observed that “interfacial strength was linearly dependent to the fourth root of welding time until it approached the bulk material strength” [11]. This information is a crucial finding for this current project because it serves as the foundation for the fundamental governing principles and correlations between weld time and weld strength. Using models based on reptation theories, the interfacial strength of lap shear welds was estimated based on thermal histories. In more detail, the activation energy for interfacial healing and self-diffusion coefficient were calculated based on shear strength measurements of samples welded with well-defined thermal histories. The parameters were then used to predict interfacial strength with varying temperature histories [11]. This provides

another major contribution because with this information it is possible to calculate an interfacial healing activation energy value.

Jud *et. al.* has observed in his studies a linear relationship between fracture toughness and the fourth root of time. He also found that samples that were healed or welded at a higher temperature required less time to achieve the same toughness [12].

Based on the studies of ultrasonic welding and impulse welding of PLA films and their characterization and activation energy calculation analyses, the current project will predict interfacial healing activation energy for various welding processes for rigid PLA samples. Currently, no heat flow models or weld strength predictions have been completed for bioplastics, such as the commercial grade of PLA 2003D, although previous studies have provided the groundwork for the theoretical approach of the models. Previous results will also help laying out how to predict temperature fields and how to incorporate this into different heat models via first order governing equations.

## **1.5 Objectives**

The objectives of this study were to:

1. Develop a molecular healing model that allows time/temperature histories to be used to accurately predict weld strengths
2. Couple molecular healing models with thermal models based on measured interfacial healing activation energy values
3. Validate the developed models with experimental data

## 1.6 References

1. Fresneau, F., De La Condamine, C.M. *Memoires de L'Academie Royale de Sciences*. 319. 1751.
2. Macquer, P. J. *Histoire de L'Academie Royale de Sciences*. 49. 1763.
3. Loadman, J. *Tears of the Tree: The Story of Rubber-a Modern Marvel*. Oxford University Press: Oxford; New York, 336. 2005.
4. Simon, E. *Annalen*. 31, 265-277. 1839.
5. Blyth, J., Hoffman, A. W. *Annalen*. 53, 292-329. 1845.
6. Armstrong, E. F. *The Constitution of Sugars*. By Prof. W. N. Haworth, D.Sc. F.R.S. Pp.100. London: Edward Arnold & Co., Ltd., 1929. 8s. 6d. *Journal of the Society of Chemical Industry*, 48, 251-251. 1929.
7. Baekeland, L.H. *Phenol-Formaldehyde Condensation Products*. *Industrial and Engineering Chemistry*, 4(10), 737-743. 1912.
8. Seymour, F.B. *Pioneers in Polymer Science*. Dordrecht/Boston/London: Kluwer Academic Publishers. 1989.
9. Grewell, D. *Modeling of molecular healing for micro-laser welding of plastics with diffractive optical elements as spatial modulators*. *Electronic Thesis or Dissertation*. Retrieved from <https://etd.ohiolink.edu/>. 2005.
10. Stoehr, N., Baudrit B., Haberstroh, E., Nase, M., Heidemeyer, P., Bastian, M. *Ultrasonic welding of plasticized PLA films*. *Journal of Applied Polymer Science*, 132, 41351. doi:10.1002/app.41351. 2015.
11. Vogel, J. *Sealing and cutting of PLA bio-plastic*. *Graduate Theses and Dissertations*. 14131. <http://lib.dr.iastate.edu/etd/14131>. 2011.
12. Jud, K., Jausch, H.H., Williams, J.G. *Fracture Mechanics Studies of Crack Healing and Welding of Polymers*. *Journal of Materials Science*, 16, 204-210. 1981.

## CHAPTER 2

### WELDING OF PLA

Leo Klinstein, Dukane Ultrasonics, St. Charles, IL

Jeff Frantz, Branson Ultrasonics, St. Louis, MO

David Grewell and Karla Lebron, Iowa State University, Department of Agricultural and Biosystems Engineering, Ames, IA

#### 2.1 Abstract

This project focuses on the characterization of bioplastics joined with impulse heat sealing. Polylactic acid (PLA), which is typically derived from starch-rich crops such as corn, was studied. PLA films were joined with impulse welding. A characterization of the mechanical properties of this bio-based plastic was completed with a tensile test to determine which welding parameters were the most influential on the weld strength. In reference to impulse welding of films, heating time and temperature were the dominant welding parameters relative to weld strength. In addition, the interfacial healing activation energy was calculated in order to predict interfacial healing for different types of welding.

#### 2.2 Introduction

Lactic acid is produced by microorganism activity that converts sugar or starch from corn and other starch-rich plants into a product that can be polymerized into polylactic acid (PLA) [1]. This biopolymer had its beginnings in the early 1800s, when a low molecular weight PLA was synthesized by Pelouze, and in 1997 Cargill and Dow Chemical formed a joint venture to create Nature Works to commercialize large-scale production of PLA, known as Ingeo. In 2007, Dow Chemical vended its 50% share in Nature Works to Teijin in Japan, who later on turned over its 50% share to Cargill, so Cargill now has sole ownership.

Polylactic acid is a brittle material with a low impact strength. These characteristics make it similar to polystyrene, which is known for its brittle qualities. In reference to tensile strength and Young’s modulus, however, it is similar to polyethylene terephthalate (PET) [2]. Polylactic acid has a lower melting temperature compared to PET and PS, as well as a lower glass transition temperature. “The CO<sub>2</sub>, O<sub>2</sub> and water permeability coefficients of PLA are lower than those of PS and higher than those of PET” [3]. Table 2.1 compares PLA’s thermo-mechanical properties to those of other polymers [4].

Table 2.1. Comparison of physical properties between PLA and commodity polymers [4].

	Properties	PLA	PS	i-PP	PET
	Relative density	1.24	1.04 - 1.06	0.91	1.37
	Clarity	Transperent	Transperent	Transperent	Transperent
Mechanical Properties	Tensile Yield Strength (Mpa)	48 - 110	34-46	21-37	47
	Tensile Modulus (Gpa)	3.5 - 3.8	2.9 - 3.5	1.1 - 1.5	3.1
	Tensile Elongation (%)	2.5 - 100	3 - 4	20 - 800	50 - 300
	Notched Izod Impact	13		72	79
Thermal Properties	Glass Transition Temperature (°C)	60	95	0	75
	Melting Temperature (°C)	153		163	250
	Vicat temperature (°C)	55 - 60	84 - 106	80 - 140	74 - 200
	Processing temperature (°C)	210	230	225	255

Recently, new methods for polymerization were reported that have allowed for a more cost-effective production of relatively high molecular weight PLA. These discoveries have been encouraged by the public’s environmental awareness and have opened up new applications for PLA. One of the benefits of PLA is that it is biodegradable in a commercial composting environment and it potentially offers a partial solution for solid waste disposal

issues and reduces the dependence on petroleum based plastics [5]. Unlike petroleum based polymers, PLA production sequesters carbon dioxide in the feedstock [6]. The variety grades of PLA are created depending on the purity and the molecular weight of the PLA as well as its molecular configuration. The composition of the PLA affects the melting point and the rate of crystallization [2].

Polylactic acid can be processed using common thermoplastic processes such as extrusion, injection molding, thermoforming, blow molding, blown film extrusion, and foaming. Examples of PLA products include extruded sheets for thermoformed products, bi-axially oriented films, blow molded bottles, injection molded products, and fibers for apparel and nonwovens [6]. For many applications, joining of subcomponents is often necessary. A common method for joining plastic films is impulse welding.

During impulse welding, one or more electrically heated elements are put in close contact with the film surfaces that need to be welded until they melt and bond at the faying surfaces. Temperature and time determine the quality of the obtained weld, which makes them the most important and influential parameters. Impulse welding machines normally use a nickel–chromium heating element that heats up when current is applied [7]. Heating times can be as short as 2 seconds, and when enough heat is applied to produce the weld, the energy is stopped and residual heat is absorbed into plastic and welding head.

This welding method was chosen because it can ultimately be used for molecular diffusion models and to calculate an activation energy that can be used to predict weld strength. Following the work by R. Wool and Loos, it is possible to measure the interfacial healing of PLA grades [11].

The following sections detail the calculation of activation energy and how this relates to the molecular diffusion process and future molecular healing models, as well as the weldability of PLA when using impulse welding, while determining which parameters are most influential to the welding process and tensile strength of the material [8].

## **2.3 Materials and Methods**

The materials studied were Ingeo 4032D and 2003D, both PLA and both manufactured by NatureWorks.

### **2.3.1 Ingeo™ biopolymer 4032D**

Ingeo 4032D is a bi-axially oriented film that can be used at temperatures as high as 300 °F (150 °C). Also, “this film has excellent optics, good machinability and excellent twist and dead fold” [9]. Ingeo 4032D is available in pellet form and is stable in the molten state.

### **2.3.2 Ingeo™ biopolymer 2003D**

Manufactured by NatureWorks and injection molded by Dukane Ultrasonics. The Ingeo biopolymer 2003D is a thermoplastic resin from renewable resources and is a “transparent general purpose extrusion grade that is used naturally or as part of a formulated blend” [10]. This material can be processed easily by extrusion to create a high molecular weight biopolymer grade PLA.

### **2.3.3 Impulse welding for molecular healing measurements**

The impulse welding system used was a customized Branson 2000 actuator (Figure 2.1) with modifications, including mounting an impulse head on the base and carriage. The design was based on water-cooling of the welding heads immediately after the heating cycle was completed. The water cooling channels were placed as near to the heating element (0.050" (1.3 mm)) as possible, while still maintaining structural integrity of the welding head. Similar



to the commercial impulse welding system, an American International Electric AIE 350FD model, heating from both sides (top and bottom) was used to reduce heating times. The heating element was a 5 mm wide nickel-chromium band and Kapton tape was used as a release agent between the heating elements and samples. Springs (tension springs) were also added to ensure that the heating element was maintained under tension despite thermal expansion during weld.

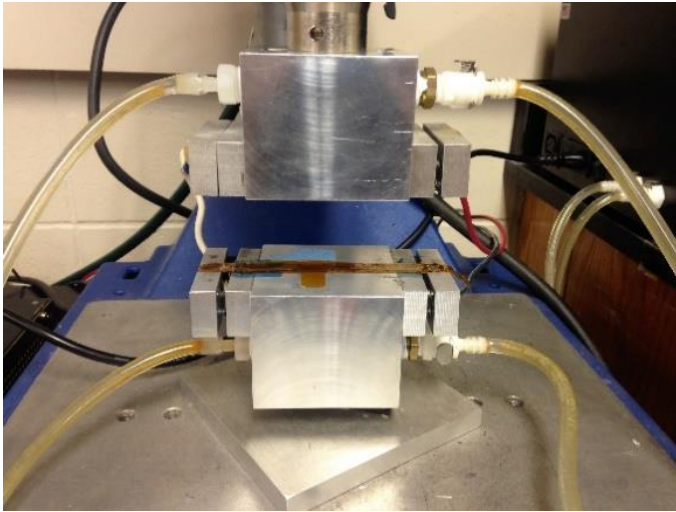


Figure 2.1. Impulse welder with heated elements on top and bottom fixtures.

The power supply box controlled the voltage and amperage, which transferred the heat into the impulse sealers on the fixtures. A constant current DC power supply (Xantrex XFR-40-70, max. current: 40 amp, max. voltage: 70 V) was used to supply electrical power to the heating elements. The upper and lower electrodes were attached in series. A Polyscience Recirculator 340 water chiller was used to regulate water flow. Relay timers, solenoid, and remote control inputs on the DC power supply were used to control the system.

In order to account for the slight delay in cooling of the joint interface caused by thermal conduction through the welding head, heating element and release agent (Kapton tape),

the water cooling was solenoid and was activated 0.5 s before the heating current was discontinued. A relay controller also allowed adjustments to the welding times.

The welding times chosen for this experiment were 2, 3, 5, 7, 25, 50, 99, 180, and 300 seconds, while the hold time remained constant at 3 seconds. The currents selected were as follows: 10, 11, 12, 13, 14, 16, and 16.7 Amps. In order to characterize this welding process, a 36-gauge thermocouple (TC) type-K wire was positioned at the corner of the seal, and then the input was recorded by a digital data acquisition system (DAQ), with a sampling rate of 10 kHz. Five replicate welds for completed for each weld time.

#### **2.3.4 Tensile testing**

Tensile testing of the impulse welded samples was completed using an Instron tensile testing system. Customized clamps were built to firmly grasp the top and bottom edges of the film samples and allow for an even distribution of force pulling up during the tensile test. For the impulse welded films, ASTM D 638 was used to define the sample geometry and weld area of 25.4 mm × 25.4 mm from the film overlap, while ASTM 3163 was followed to complete testing in a lap shear joint configuration. Films with a lap shear configuration with an overlap of 25.4 mm were welded and tested using an Instron. The sample geometry had to be modified for the Instron, with a 5 kN load cell and a crosshead speed of 10 mm/min. Sample data collected from tensile testing was the ultimate stress. Customized grips designed to test film were used to avoid slippage and tearing of the film.

## 2.4 Results and Discussion

### 2.4.1 Impulse welding

In Figure 2.2 and Figure 2.4, the weld factor is the “failure load of the welded samples divided by the failure load of the base material” [7]. Once the weld factor was calculated for each weld time at the selected current values and corresponding temperatures, it was plotted as a function of weld time to the 1/4<sup>th</sup> power in order to obtain the y-intercept equation for each line. The slope of the equation for each line is plotted in Figure 2.3 and Figure 2.5 as a function of the inverse temperature. From this plot a line can be drawn, and then the slope of the line is taken to calculate the activation energy.

The Arrhenius law is rewritten as:

$$K(T) = K_0 \cdot \exp\left[-\frac{E_a}{kT}\right] \quad (1)$$

$K(T)$  – Product of proportionality constant times the self-diffusion coefficient and dimensionless

$E_a$  – Activation energy with units of Joules

$K_0$  – Constant and dimensionless

$k$  – Boltzmann constant

$T$  – Absolute temperature

The parameters  $K_0$  and  $E_a$  were determined by plotting the natural log (ln) of the slopes of the curves versus the inverse temperature. The slope determines the value of  $E_a$  while the intercept determines the value of  $K_0$ . The slope is then multiplied by an R constant and then

the true activation energy is calculated. For the Ingeo 2003D the  $E_a$  is 1.79 kJ/mol with a  $K_o$  of 2.40, and for the Ingeo 4032D the  $E_a$  is 17.6 kJ/mol with a  $K_o$  of 343.

It can be shown experimentally that tensile strength increases in proportion with the weld time to the  $1/4^{\text{th}}$  power. The bonding is more difficult to achieve at the lower temperatures because of insufficient durations of weld time, and chain fracture at higher temperatures will cause an increase in the failure load for longer weld times.

In Figure 2.2 and Figure 2.4, the error bars correspond to a  $\pm 1$  standard deviation. Samples tested from the impulse welding machine showed a relationship between weld time and temperature. The lowest temperature for the Ingeo 2003D results at  $86^\circ\text{C}$  shows a need for longer welding times compared to the highest temperature ( $180^\circ\text{C}$ ), which benefits from shorter welding times.

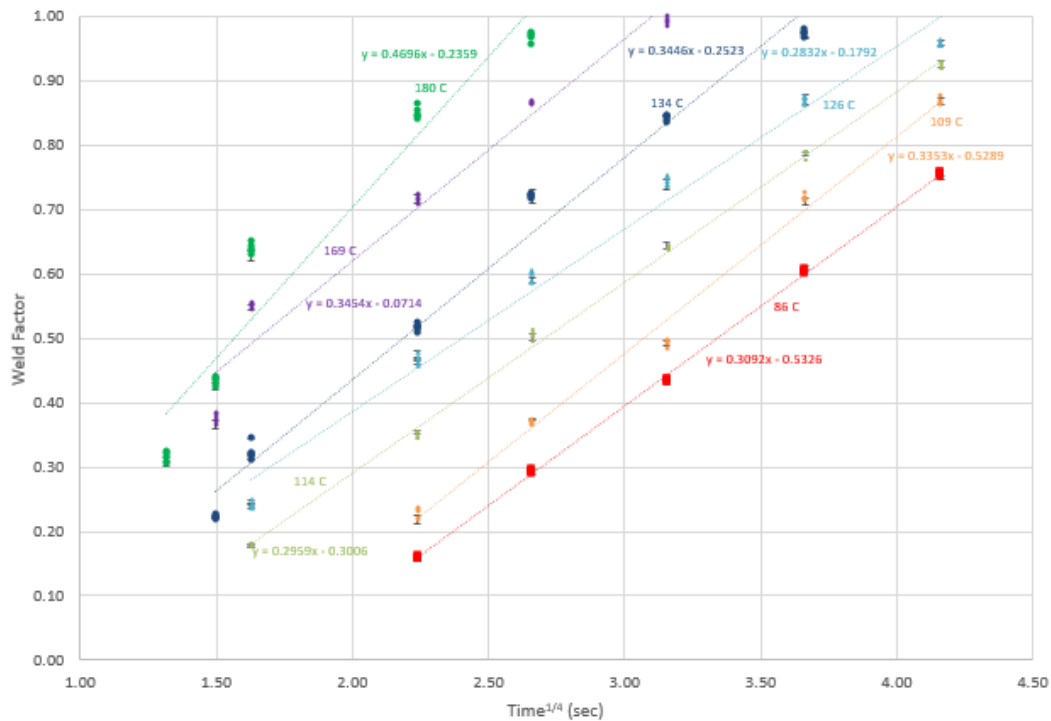


Figure 2.2.  $\text{Time}^{1/4}$  as a function of weld factor (Ingeo 2003D).

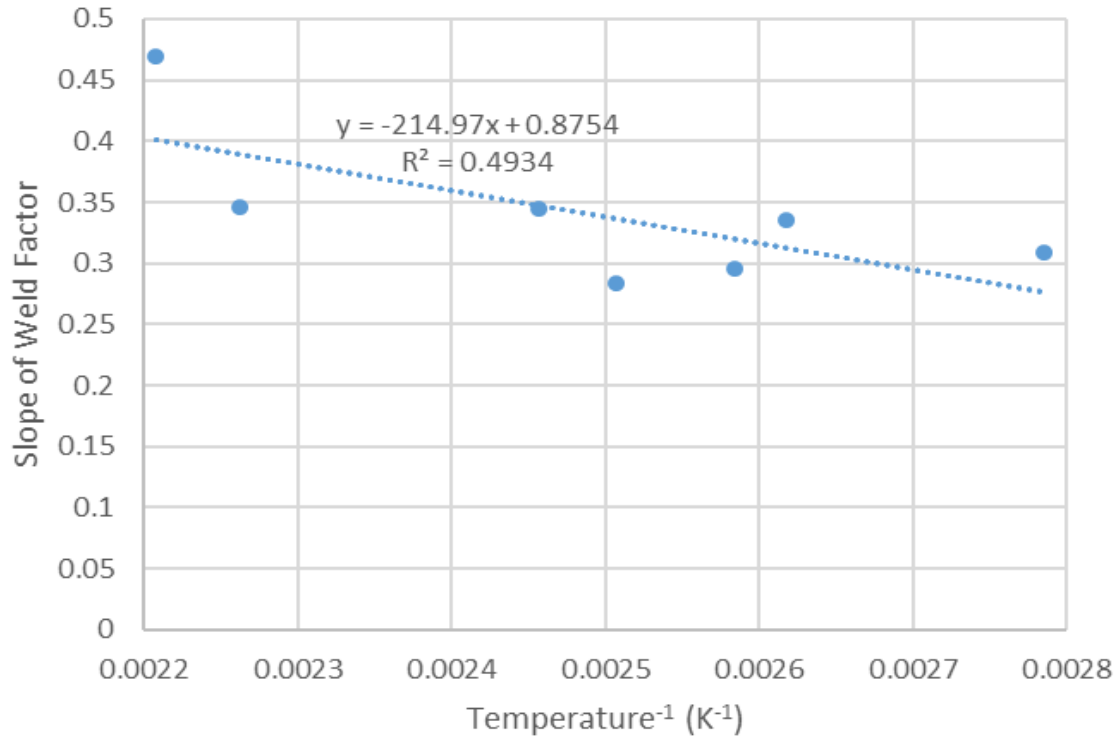


Figure 2.3. Temperature<sup>-1</sup> as a function of slope of weld factor (Ingeo 2003D).

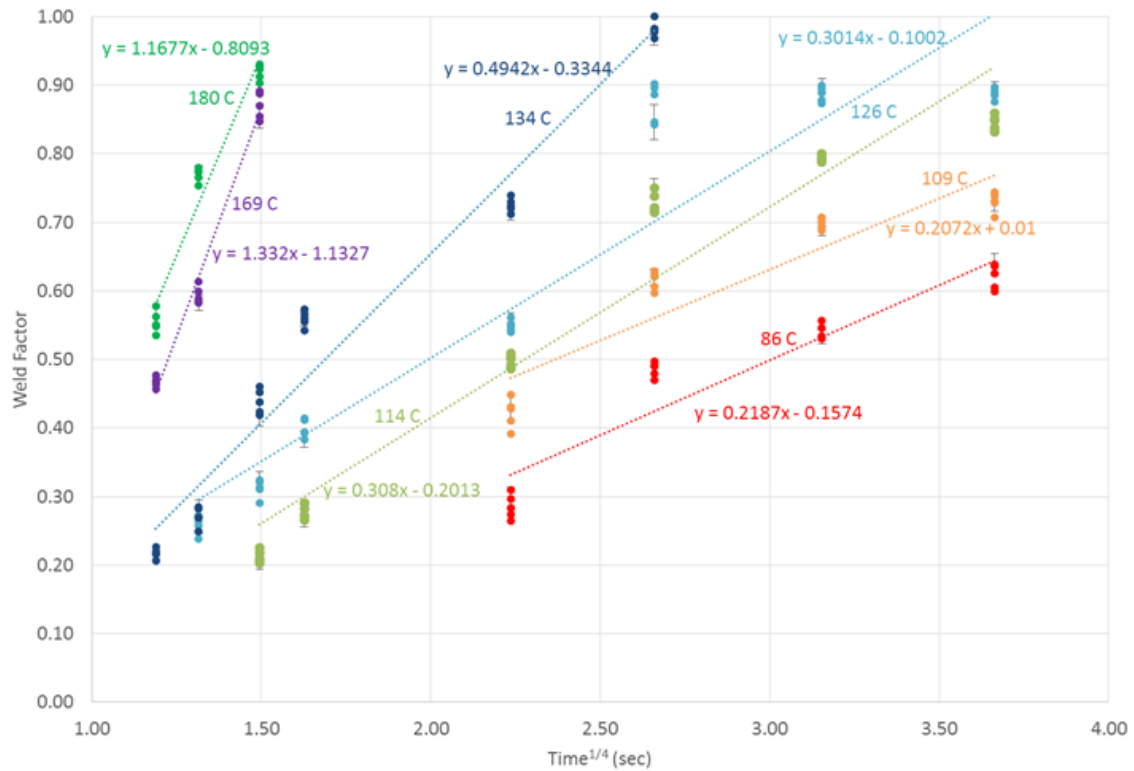


Figure 2.4. Time<sup>1/4</sup> as a function of weld factor (Ingeo 4032D).

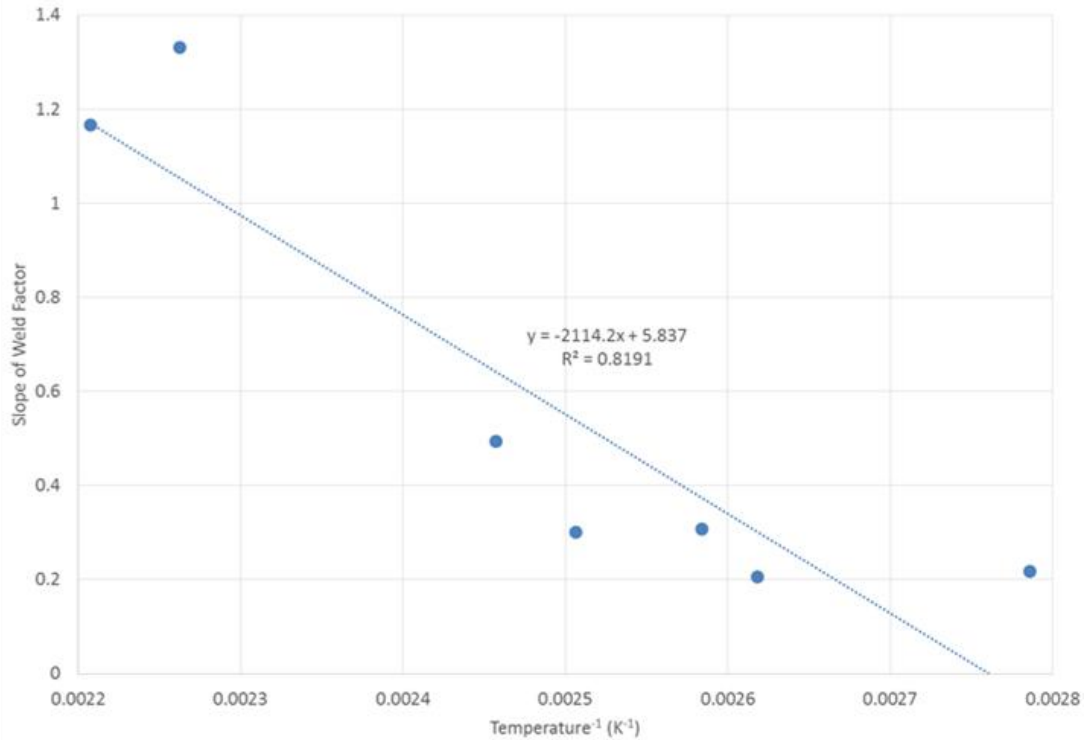


Figure 2.5. Temperature<sup>-1</sup> as a function of slope of weld Factor (Ingeo 4032D).

## 2.5 Conclusion

From the samples tested for impulse welding, it was seen that increasing the weld time for the lower current values caused the weld factor to increase. In addition, when the weld time was decreased for higher current settings, the weld factor approached 1. In general, with excessive weld energy, relatively long heating time with relatively high current values, the films were damaged and relatively low weld strengths were seen. Impulse welding can yield good results for weld times starting as low as 25 seconds, and as high as 300 seconds.

The activation energy calculation which resulted in  $E_a = 1.79$  kJ/mol for the Ingeo 2003D, and in  $E_a = 17.58$  kJ/mol for the Ingeo 4032D. Ultrasonic welding on PLA rigid samples show that weld distance and weld velocities affect the ultimate stress experienced during the tensile test. In general, weld strength is proportional to weld distance and inversely proportional to weld/melt velocity.

## 2.6 References

1. Garlotta, D. *Journal of Polymers and the Environment*, 9, 63-84. 2001.
2. Sin, L.T., Rahmat, A.R., Rahman, W.A.W.A. *Polylactic Acid - PLA Biopolymer Technology and Applications*, Elsevier. 2012.
3. Auras, R., Harte, B., Selke, S. *Macromolecular Bioscience*, 4, 835–864. 2004.
4. Carrasco, F., Pagès, P., Gámez-Pérez, J., Santana, O.O., MasPOCH, M.L. *Polymer Degradation and Stability*, 95, 116–125. 2010.
5. Lim, L.T., Auras, R., Rubino, M. *Progress in Polymer Science*, 33, 820–852. 2008.
6. Hopmann, C., Schippers, S., Höfs, C. *Journal of Applied Polymer Science*, 132, 41532. 2015.
7. Vogel, J., Grewell, D., Kessler, M., Drummer, D., Menacher, M. *Ultrasonic and impulse welding of polylactic acid films. Polymer Engineering and Science*, 51, 1059–1067. 2011.
8. Farrington, D.W., Lunt, J., Davies, S., Blackburn, R.S. *Biodegradable and Sustainable Fibers*, Blackburn, Leeds, 192. 2005.
9. NatureWorks. Ingeo™ Biopolymer 4032D Technical Data Sheet. Retrieved from [http://www.natureworkslc.com/~media/Technical\\_Resources/Technical\\_Data\\_Sheets/TechnicalDataSheet\\_2003D\\_FFP-FSW\\_pdf.pdf](http://www.natureworkslc.com/~media/Technical_Resources/Technical_Data_Sheets/TechnicalDataSheet_2003D_FFP-FSW_pdf.pdf). 2016.
10. NatureWorks. Ingeo™ Biopolymer 2003D Technical Data Sheet. Retrieved from [http://www.natureworkslc.com/~media/Technical\\_Resources/Technical\\_Data\\_Sheets/TechnicalDataSheet\\_4032D\\_films\\_pdf.pdf](http://www.natureworkslc.com/~media/Technical_Resources/Technical_Data_Sheets/TechnicalDataSheet_4032D_films_pdf.pdf). 2016.

**CHAPTER 3****DEVELOPMENT OF MOLECULAR DIFFUSION MODELS FOR  
ULTRASONIC WELDING OF PLA**

Leo Klinstein, Dukane Ultrasonics, St. Charles, IL

Jeff Frantz, Branson Ultrasonics, St. Louis, MO

Karla Lebron †, David Grewell †

†Department of Agricultural and Biosystems Engineering  
Iowa State University

To be submitted to Polymer Engineering and Science

**3.1 Abstract**

This paper focuses on the characterization of bioplastics joined using ultrasonic welding and modeling of temperature distributions and interfacial healing. Polylactic acid (PLA), which is typically derived from starch-rich crops such as corn, was studied. While the measurement of activation energy for interfacial healing at weld interfaces of PLA films has been reported, here, this information is used to predict the weld strength of rigid PLA samples welded by ultrasonics [1]. A characterization of the mechanical properties was completed with a tensile test to determine the effects of amplitude, melt velocity and collapse distance on weld strength. From previous interfacial healing activation energy measurements based on an impulse welding method, it was also possible to predict weld strength.

It was found that the most influential parameters were weld time, collapse distance and weld velocity. In general, the model predicted weld strength reasonably well with  $r^2$  values between 0.77 and 0.78.



## 3.2 Introduction

### 3.2.1 Ultrasonic welding

For many applications, joining of subcomponents is often necessary. A common method for joining plastics is ultrasonic welding. Ultrasonic welding joins parts by using mechanical vibrations. These vibrations are applied to the parts via a sonotrode (horn) and cause the material to melt (be plasticized) and join the part surfaces that are in contact. A force is applied to the parts by the horn that vibrates at frequencies typically between 20–40 kHz, at relatively low amplitudes 50–200  $\mu\text{m}$  p-p [2]. Ultrasonic welding is a common welding technique in industry because of its short cycle time – typically less than a second. While single ultrasonic systems are limited by size, it is possible to weld large assemblies by using multiple systems simultaneously.

“Usually a designed asperity is molded into one of the parts to improve the consistency of heating and welding. This protrusion, which is also called an energy director or concentrator, experiences the highest levels of cyclical strain producing the greatest level of heating. Therefore, the energy director melts and flows to join the parts” [2]. The ultrasonic welding equipment “consists of a converter or transducer, booster and the sonotrode or horn” [3].

It has been reported that it is possible to measure the interfacial healing of PLA grades following the work by R. Wool and Loos [4, 5]. In addition, it has been reported that it is possible to predict weld strength of complex varying temperature welds, such as those seen in heat-sealing. In addition, it has been demonstrated that by segmenting the complex temperature histories into small constant temperature approximations and summing the degrees of welding, it is possible to predict the final weld strength [6].

This work details the weldability of PLA when using ultrasonic welding and determines the effects of the various welding parameters on strength. Building on previous work based on fundamental governing equations, this paper will compare predicted weld strength of ultrasonic welding to experimental data to validate the novel model developed in this paper.

### 3.2.2 Molecular healing

Healing of polymer interfaces occurs when, in this study's case, two faying surfaces make contact at an elevated temperature. This means that polymer chains are able to diffuse across the interface. The healing process can be seen in Figure 3.1 for various levels of healing [2]. When there is complete healing, the polymer chains from the top sample part and the base part of the sample will be completely intermingled and will become one part. In this case a degree of welding (DW) is defined as 1.0.

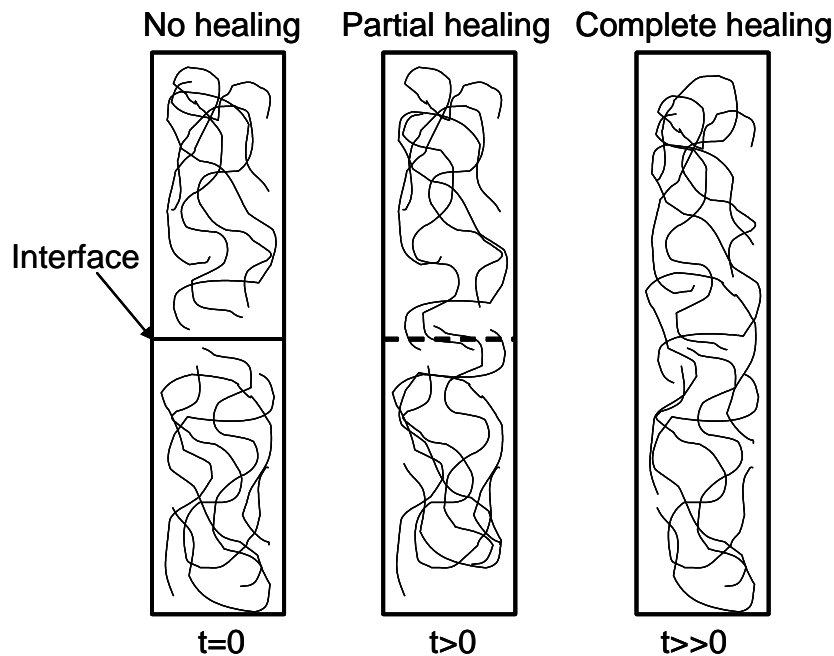


Figure 3.1. Molecular diffusion and interfacial healing.

Interfacial healing is time and temperature dependent and affected by many factors. Some of these factors include aspects regarding the polymer base material such as the

molecular structure, the molecular weight, and chemical structure. Pressure can affect the time to achieve complete healing. De Gennes presented his ideas on how to model the diffusion of polymer chains by using the reptation theory [7]. His model created an imaginary tube of a certain length  $L$  in which each polymer chain would be encased. There is more mobility at the ends of the polymer chains compared to the center area of the chain because the imaginary tube is defined by constraints of neighboring polymer chains. The distance that a chain travels outside the original tube is referred to as the mean diffusion distance squared ( $\langle l \rangle^2$ ) and it can be related to time as shown in Figure 3.2 [6].

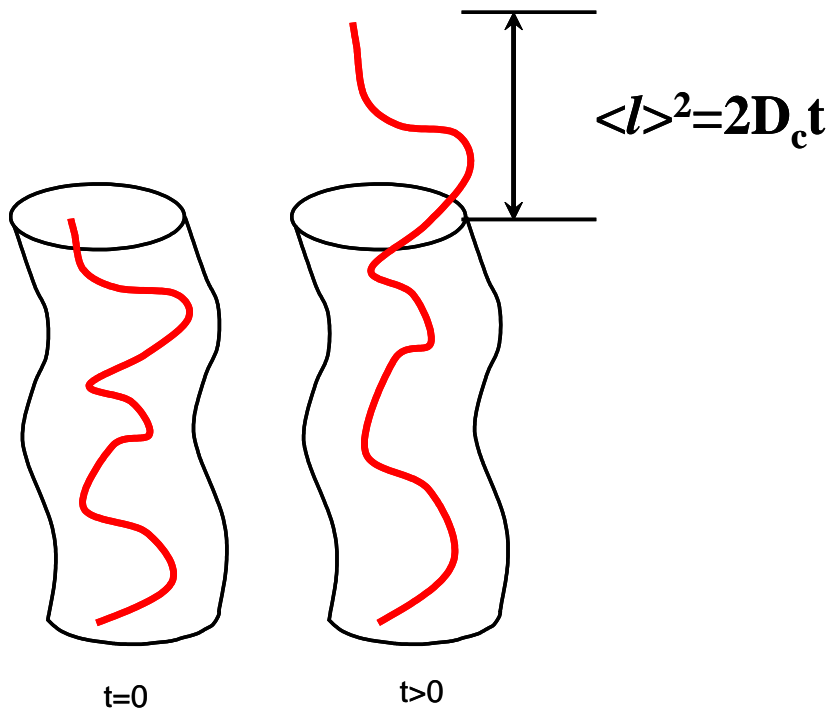


Figure 3.2. Molecular diffusion and interfacial healing and Einstein's diffusion equation.

Equation 2 depicts the relationship between the distance a chain propagates across a given interface and the mean diffusion distance squared ( $\langle l \rangle^2$ ) of any one chain near the interface [6].

$$X \approx \sqrt{\langle l \rangle^2} \quad (2)$$

Equation 3 shows how healing time is related to time by the power of  $\frac{1}{4}$ . The diffusion coefficient is noted as  $D$  [6].

$$\begin{aligned} \langle l \rangle^2 = 2Dt \Rightarrow l = \sqrt{2Dt} \Rightarrow X = (2Dt)^{\frac{1}{4}} \\ \therefore \\ X \sim t^{\frac{1}{4}} \end{aligned} \quad (3)$$

Furthermore, Equation 4 expresses Jud's propositions that the diffusion coefficient is an Arrhenius function of temperature (T) [6].

$$D(T) = D_0 e^{\left[ \frac{-E_a}{RT} \right]} \quad (4)$$

In this equation,  $D_0$  represents the diffusion constant,  $E_a$  is the activation energy and  $R$  is the Boltzmann constant ( $1.3807 \times 10^{-23}$  J/K).

This equation is applicable to a system with rapid heating and cooling temperature profile such as in impulse welding, shown in Figure 3.3. This study is based on a model from previous work to estimate the interfacial activation energy of PLA.

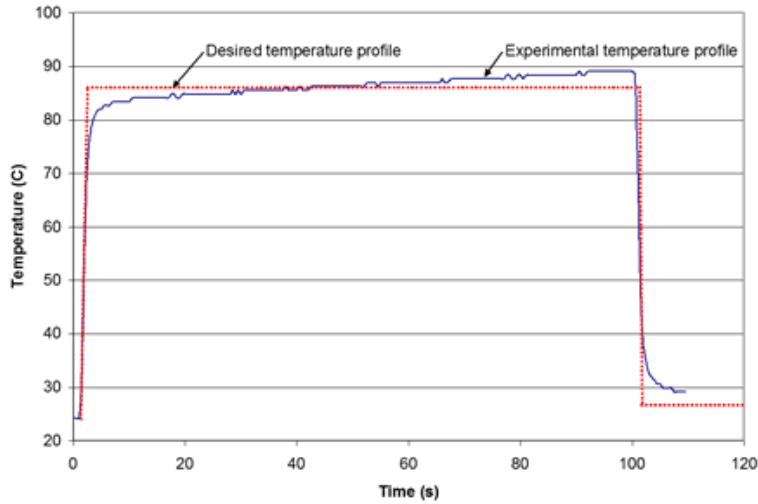


Figure 3.3. Details impulse welding temperature profile.

In more detail, it was previously reported that the temperature profile for impulse welding at different times and temperatures can be used to estimate a temperature independent interfacial healing activation energy. However, it is possible to section complex thermal models (“non-top hat”) into small time increments, as shown in Figure 3.4, in order to get a summation of all the autohesions and to estimate the total degree of weld (DW).

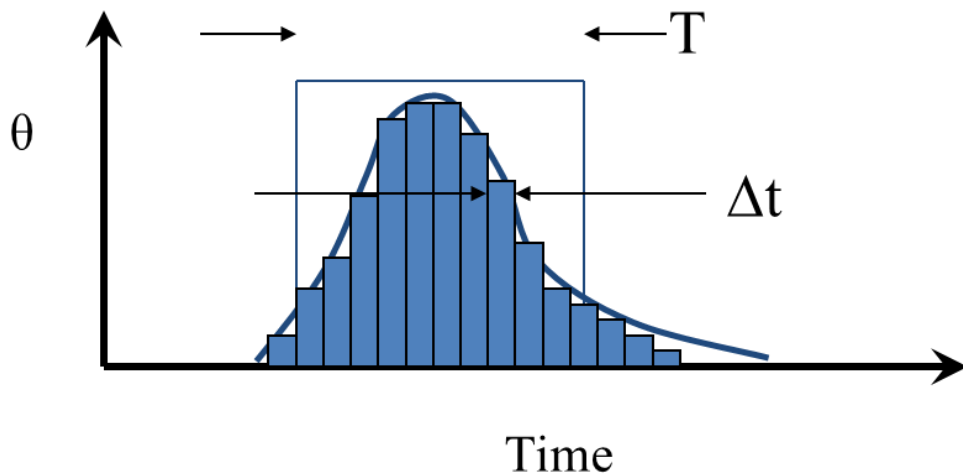


Figure 3.4. Details time increments in impulse welding temperature profile for degree of weld calculation.

The total degree of weld can be estimated utilizing Equation 5 [6].

$$DW(T, t)_h = \sum_{t=0}^{t=t'} K_0 * e^{\frac{-E_a}{RT}} * \Delta t^{1/4} \quad (5)$$

In most cases, it is assumed that activation energy is temperature-independent. Wool studied polystyrene, and he suggested that activation energy is temperature-independent [4]. However, following observations by Grewell, it was noted that the activation energy was actually temperature-dependent in the range of temperatures described in Figure 3.5 [6].

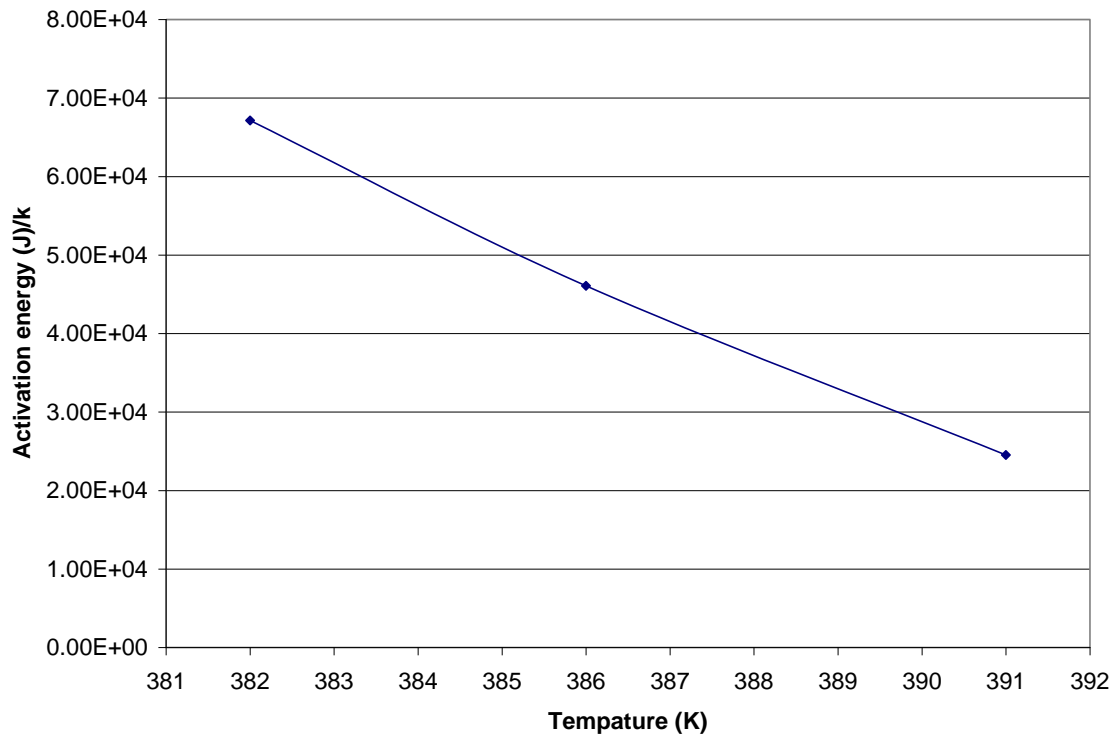


Figure 3.5. Plot of activation energy as a function for temperature for PS as report by Wool [6].

Loos and Dara studied the healing of polysulphone and assumed the activation energy to be temperature-independent [5]. Their plotted data in Figure 3.6 shows the degree of healing (autohesion) as a function of time for various temperatures.

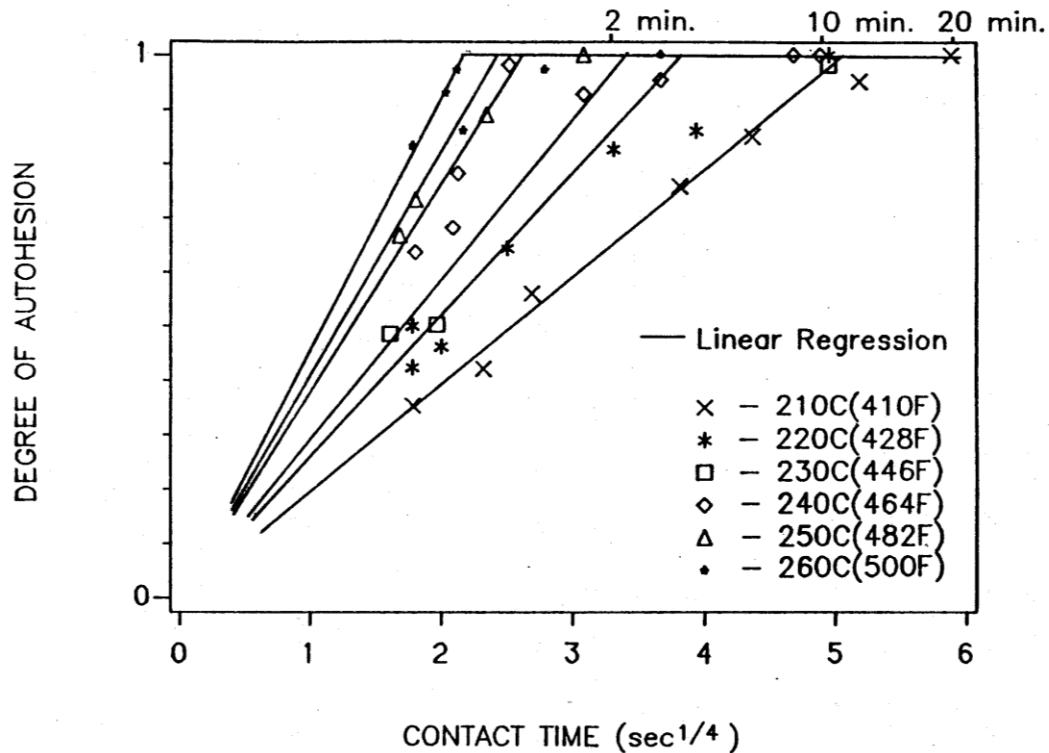


Figure 3.6. Degree of healing as a function of time for polysulphone [5].

In Figure 3.7, the natural logs of the slopes of the various temperatures are plotted as a function of the inverse temperature, and the activation energy can be estimated from the slope of this line [6]. The solid line is the slope that is assumed by Loos. While this estimate is reasonable, Grewell proposed that a better fit was the one that has a temperature-dependent slope [6]. This is shown as the dashed line in Figure 3.7.

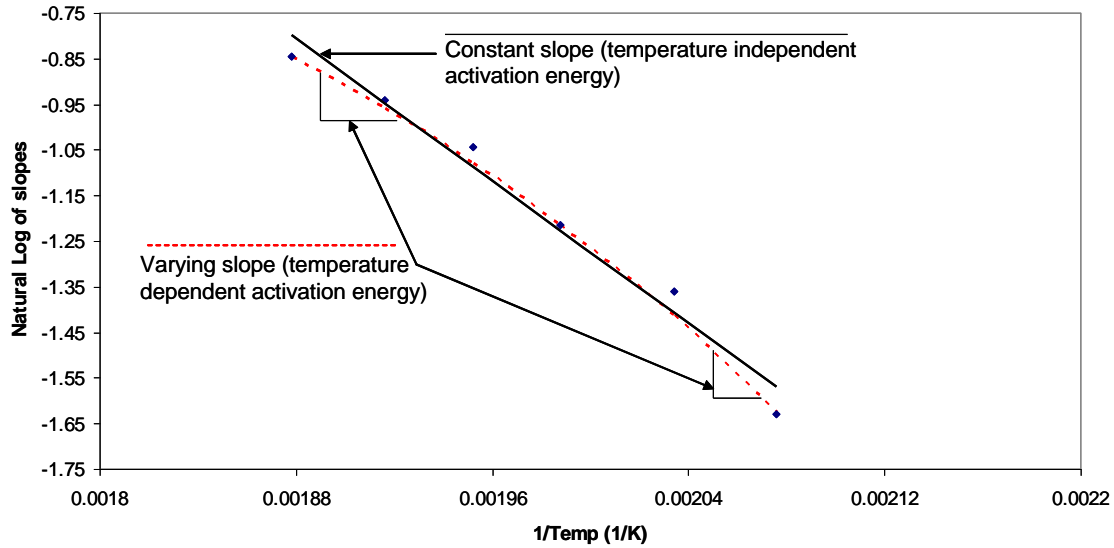


Figure 3.7. Plot of natural log of slopes of as a function of inverse temperature (polysulphone).

The assumption of a temperature-independent activation energy reported by Wool, Loos and Dara on polystyrene and polysulphone is not completely applicable for studies where the temperature is relatively high, such as the case with ultrasonic welding. When predicted temperatures go beyond the range of those used to measure the activation energy, the reported temperature independence is no longer a valid assumption at the slopes suggested by Loos. In this study of PLA, the ranges of predicted temperatures tended to be higher than what can be measured with impulse heating, which is the standard method for measuring the activation energy. In impulse welding, it is not possible to measure the activation energy above 250–300°C, as thermal inertia prevents “top hat” temperature histories from being generated. As illustrated in Figure 3.7, the predicted peak temperature in ultrasonic welding is significantly higher than the temperatures that can be studied in impulse welding. It is important to note that Grewell measured similar temperature profiles in ultrasonic welding as those seen in Figure 3.8 [8]. In addition, Grewell also reported that interfacial activation energy can be temperature-dependent [6, 8].



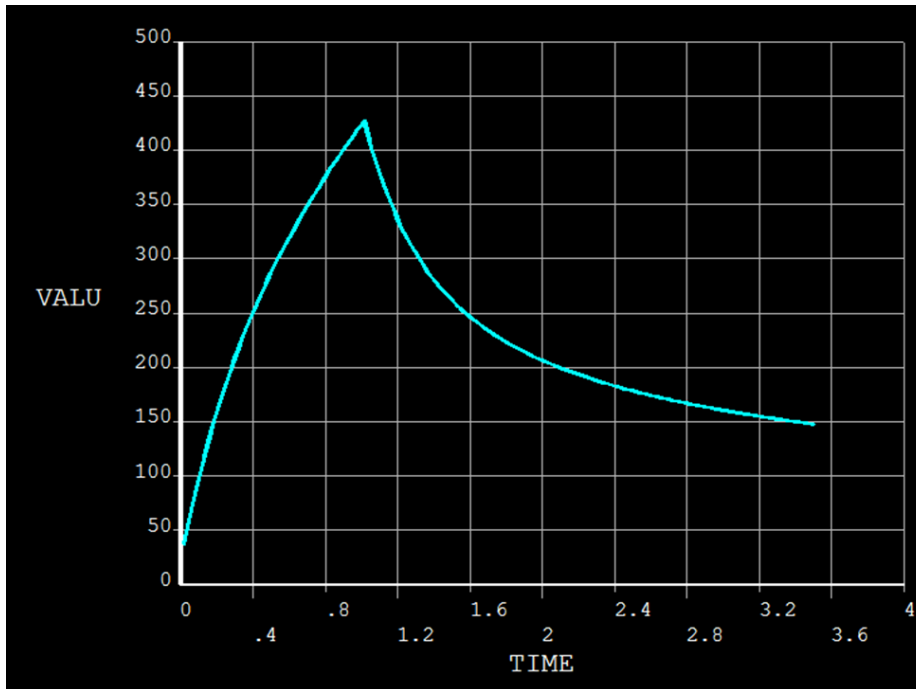


Figure 3.8. Plot of ANSYS temperature profile for collapse distance of 0.1 mm, weld velocity of 0.1 mm/s and amplitude of  $21.6 \mu\text{m}_{p-p}$ .

When the range of predicted temperatures is out of the studied range, it is justifiable that the activation energy be temperature independent and higher than the previously reported activation energy of 17.58 kJ/mol.

The temperature profiles from ANSYS were used to predict the degree of weld based on interfacial healing activation energy. The degree of weld is the summation of all autohesions of each time interval as stated in Equation 5. This degree of weld is then multiplied by the highest ultimate stress value from each collapse distance within each of the two studied amplitudes to yield a final predicted strength. While the part had a well-controlled geometry, it would be more appropriate to consider the base material as a normalizing property. Because of the complex weld design used in ultrasonic welding, there are geometric effects that greatly affect stress distribution within the weld. In order to account for these effects, it was assumed that the highest observed weld strength correlates to a nearly fully healed weld line ( $DW=1$ ).

### 3.3 Materials and Methods

#### 3.3.1 Ingeo™ biopolymer 2003D

The PLA material used was Ingeo biopolymer 2003D, manufactured by NatureWorks. It was injection molded into innovative round “Industry Standard Test Parts” (ISTeP) by Dukane Ultrasonics as seen in Figure 3.9. The samples consisted of a rigid cap and base, had a 0.5 mm tall, round energy director, a diameter of 35 mm and a wall thickness of 2.36 mm.



Figure 3.9. PLA Rigid Sample (Ingeo 2003D).

#### 3.3.2 Ultrasonic welding for molecular healing validation

The ultrasonic welding system used was a Dukane iQServo system (Figure 3.10), operating at a frequency of 20 kHz.

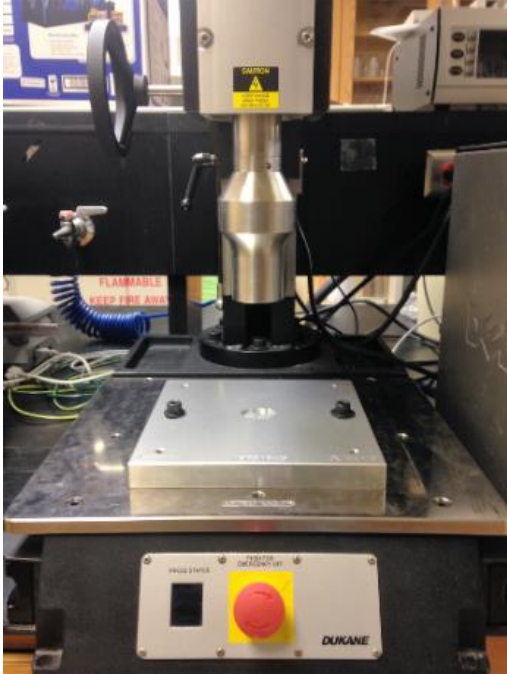


Figure 3.10. Dukane ultrasonic welder.

All experiments had the trigger force set to 300 N. Three different collapse distances were tested (0.1 mm, 0.2 mm, 0.3 mm) at an amplitude of  $21.6 \mu\text{m}_{\text{p-p}}$  and  $32.4 \mu\text{m}_{\text{p-p}}$ . The iQServo press ultrasonic system had a software, iQ Explorer II, which was used to control the welding conditions as well as the horn's motion before it comes in contact with the sample. The position at trigger was one of the conditions in this software and was the point when the ultrasonic welding horn started detecting the sample before the ultrasonic energy was engaged. The collapse distance, which is assumed to be the distance the parts melted together, was then added to this position at trigger in order to obtain the total horn distance traveled.

Based on screening experiments, collapse distances of 0.1 mm, 0.2 mm, and 0.3 mm were chosen, with a sensing speed of 0.300 mm/s. The sensing speed indicated the rate at which the horn moved down to detect the sample once the position at trigger was reached. An illustration of this sonication process can be seen in Figure 3.11, where the position at trigger and sensing speed fall under the pre-weld phase [9]. Likewise, Figure 3.12 details phases of

the welding cycle as seen on the iQ Explorer II software, with phase 3 demonstrating the difference in collapse distance [9].

It is important to note the following:

1. Once the Trigger Force (set at 300 N per recommendations on part design and application requirements) is reached, the motion stops and sonication is activated.
2. Position is maintained until the force drop or Melt-Detect™ (programmable value) is reached.
3. Motion resumes with the programmable velocity profile until the weld condition is reached (Collapse Distance, Weld Energy or Peak Power), at which point sonication is turned off.
4. The position is maintained for the Static Hold time.

The purpose is to provide extra squeeze to prevent shrinkage.

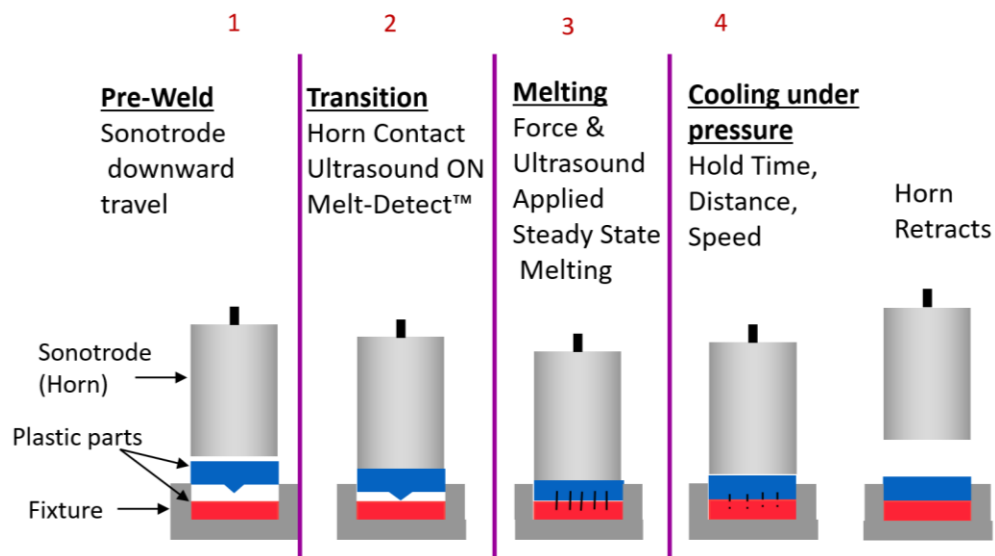


Figure 3.11. Phases of the ultrasonic welding cycle.

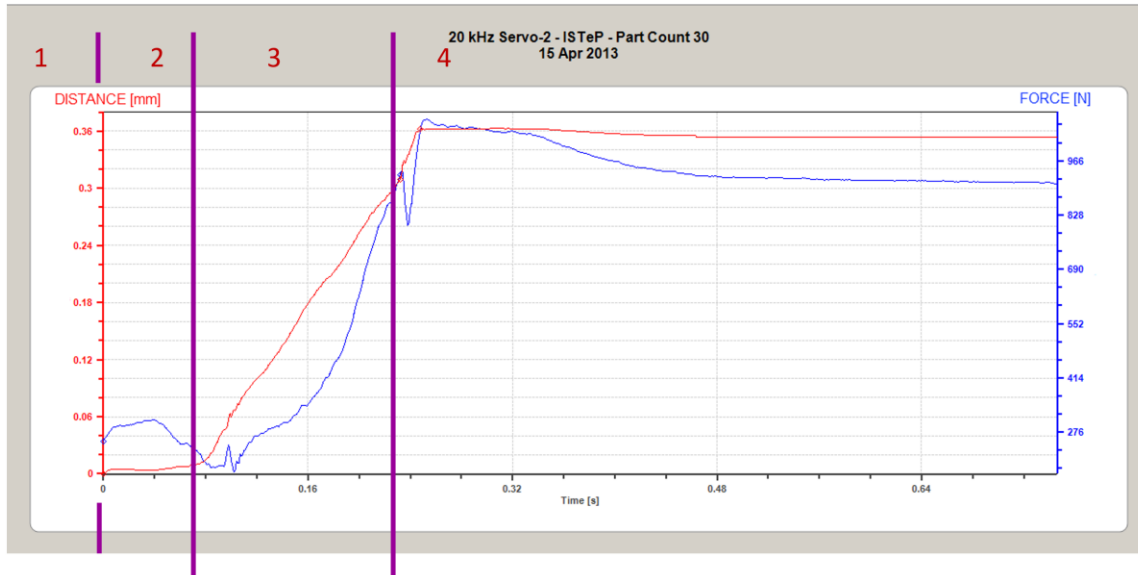


Figure 3.12. Phases of welding cycle as seen on iQ Explorer II software.

In addition to the three collapse distances (0.1 mm, 0.2 mm, and 0.3 mm), six different welding velocities were examined (0.1 mm/s, 0.2 mm/s, 0.4 mm/s, 0.6 mm/s, 0.8 mm/s, 1 mm/s) for each weld distance as seen on Table 3.1. The welded samples were replicated three times using a  $2 \times 3 \times 6$  experimental design.

Table 3.1. Welding parameter used for molecular diffusion design of experiments for  $21.6 \mu\text{m}_{p-p}$  and  $32.4 \mu\text{m}_{p-p}$  amplitude.

Sample	Weld Velocity (mm/s)	Weld Distance (mm)
A1	0.1	0.1
A2	0.2	0.1
A3	0.4	0.1
A4	0.6	0.1
A5	0.8	0.1
A6	1	0.1
B1	0.1	0.2
B2	0.2	0.2
B3	0.4	0.2
B4	0.6	0.2
B5	0.8	0.2
B6	1	0.2
C1	0.1	0.3
C2	0.2	0.3
C3	0.4	0.3
C4	0.6	0.3
C5	0.8	0.3
C6	1	0.3

For clarification, there were seven major task/experiments conducted as detailed in Figure 3.13.

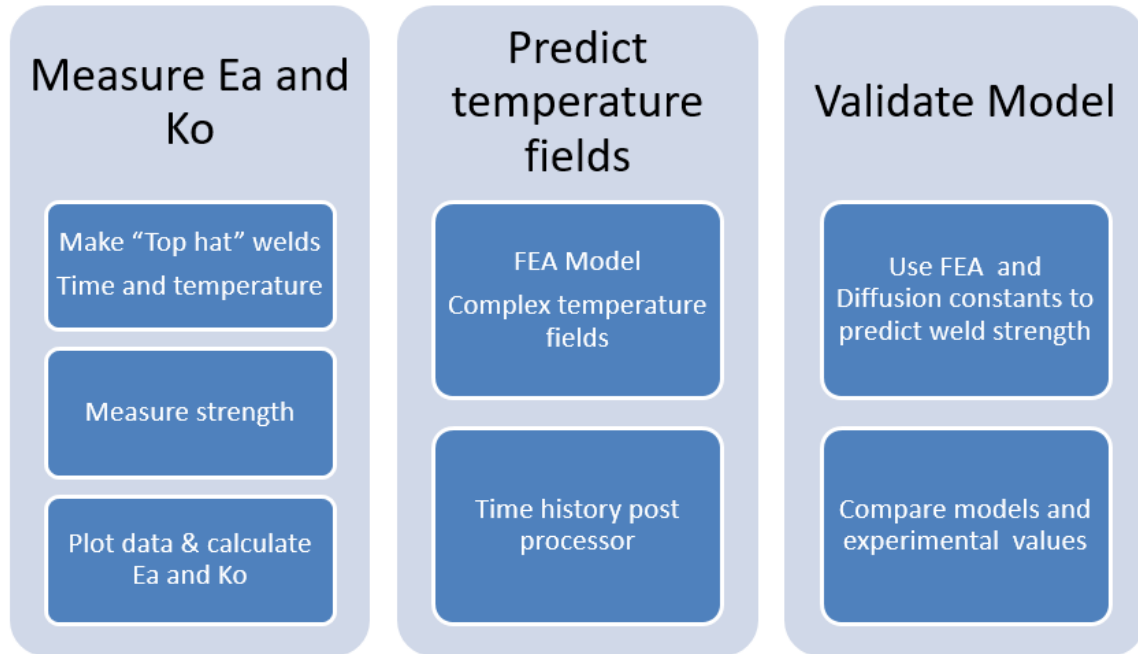


Figure 3.13. Summary of molecular healing model development and verification.

### 3.3.3 Tensile testing

Tensile testing of the ultrasonic welded samples was completed using an Instron tensile testing system. Customized clamps were built to firmly grasp the top and bottom edges of the cylindrical rigid sample and allow for an even distribution of force pulling up during the tensile test. This test was performed at a crosshead speed of 3 mm/min, and the weld area was determined by applying the inside radius,  $r_1$ , and the outside radius,  $r_2$ , of the round hollow cylinder sample to Equation 6.

$$A_w = \pi (r_2 - r_1)^2 \quad (6)$$

The Instron's output was the measurement for weld strength, which was ultimate stress.

### 3.3.4 FEA modeling with ANSYS

FEA Model: ANSYS is a structural analysis software that enables the ability to solve complex structural engineering problems, facilitating better and faster design decisions. With the finite element analysis (FEA) tools available, solutions can be customized for any discipline, and these tools are used throughout the industry to enable engineers to optimize their product designs and reduce the costs of physical testing. In this study, the finite element analysis application of thermal analysis was utilized in order to predict transient temperature fields. These temperature fields allowed for the development of molecular diffusion modeling as well as for the determination of predicted weld strengths when using a predetermined activation energy. The primary assumptions were made.

Assumptions:

1. Isothermal conditions
2. Semi-infinite body
3. Constant material properties
4. No phase changes
5. Calculated heat flux was distributed to both sides of the volume of elements created
6. Heat flux is set as a boundary condition at the faying surface
7. Analysis only considers conduction term
8. Negligible convection term
9. Refinement of elements is limited to the surface of the volume because this is where the thermal gradient occurs and it saves time

The volume and element type (Solid Brick 8node 70) for the finite element analysis are shown in Figure 3.14.

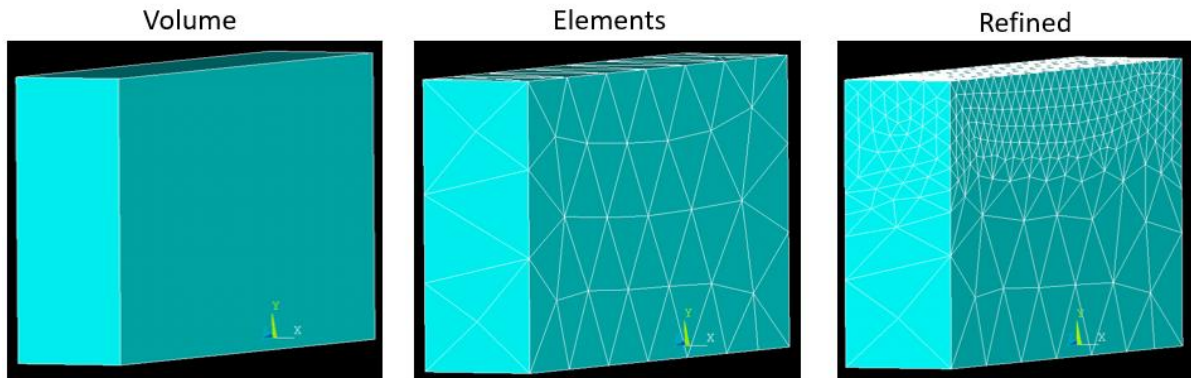


Figure 3.14. ANSYS volume (left), volume divided into elements through meshing function (center), and elements refined (right).

Using the heat generation model, a finite element model was produced using ANSYS. There were two-step load options in the model. Load step option 1 corresponded to the heating with heat flux (based on power reported from the power supply during experimental results) for a predetermined weld time portion. Load step option 2 consisted of discontinuing the applied heat followed by cooling. The time step for this load steps was 0.2 seconds.

Material properties included a density ( $1189 \text{ kg/m}^3$ ), specific heat ( $1500 \text{ J/kg}\cdot\text{K}$ ), and thermal conductivity ( $0.18 \text{ W/m}\cdot\text{K}$ ). The model included conduction and convection terms; however, it should be noted that the convection term could be ignored, as its effects were negligible as seen from the thermal gradients at the edge of the sample at the part/air interface.

A comparison of Figure 3.15 and Figure 3.16 illustrates the negligible effects of the convection term. Figure 3.15 did not consider the convection term, while Figure 3.16 shows the thermal gradient with the convection term.

Both figures exhibited near identical minimum and maximum temperatures in the finite element analysis model.



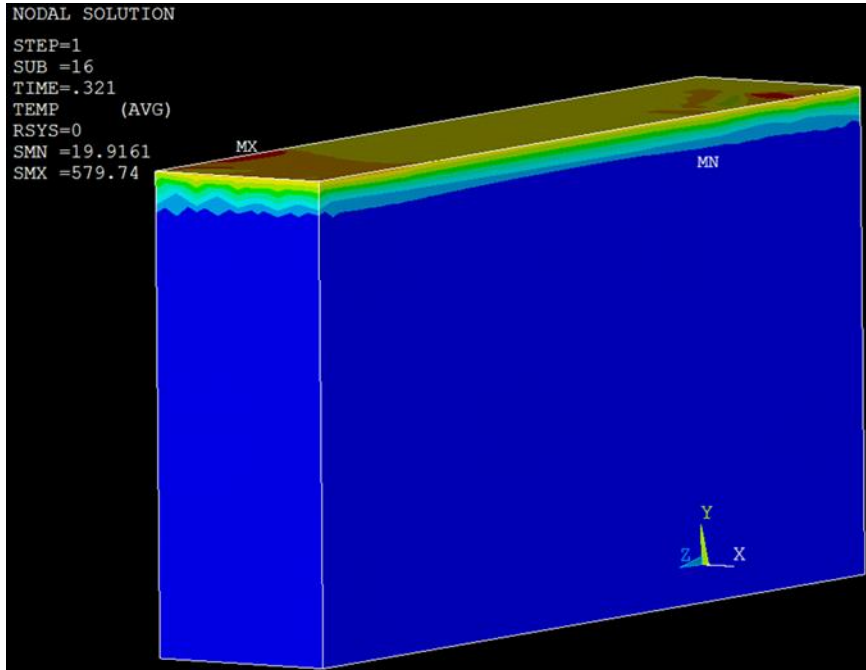


Figure 3.15. ANSYS thermal gradient without convection for collapse distance of 0.3mm, weld velocity of 1mm/s and amplitude of  $21.6 \mu\text{m}_{p-p}$  (Sample C6).

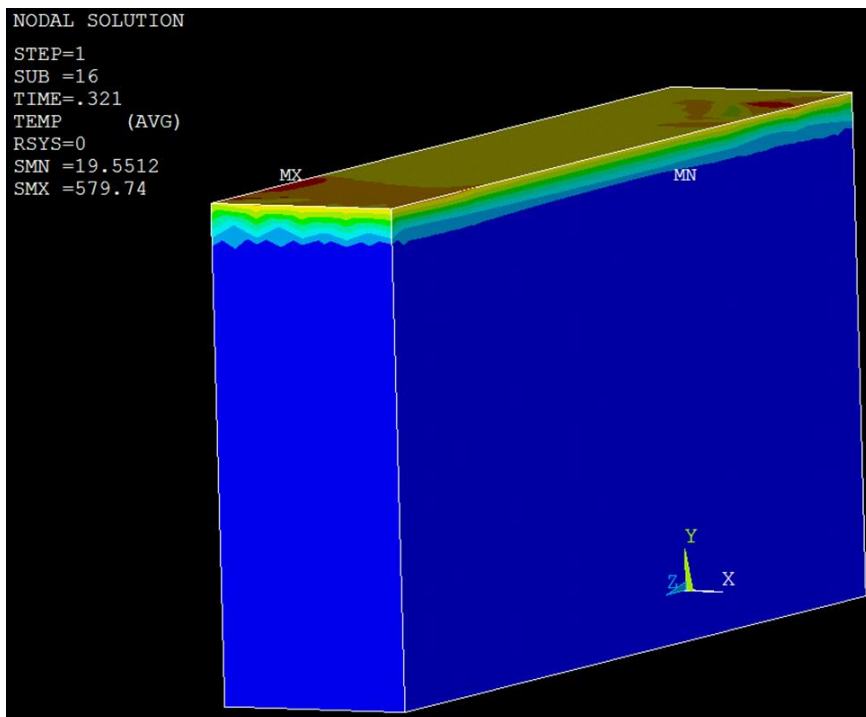


Figure 3.16. ANSYS thermal gradient with convection for collapse distance of 0.3mm, weld velocity of 1mm/s and amplitude of  $21.6 \mu\text{m}_{p-p}$  (Sample C6).

### 3.3.5 Heating model

In general, the heat source model included a number of aspects:

1. The average power reported by the welding power supply was assumed to be the actual energy dissipated for a given set of welding parameters.
2. Using a sub-set of data from #1, the loss modulus ( $E''$ ) for PLA was estimated based on the geometry of the weld as well as the amplitude.
3. Based on the dissipated average power ( $W$ ) for a given set of welding parameters (#1), a heat flux ( $W/m^2$ ) was estimated based on weld area ( $m^2$ ).
4. Based on the heat flux (#3) and a transient thermal model with finite element analysis, FEA was developed.
5. Based on the effective loss modulus ( $E''$ ), the volumetric heating rate ( $W/m^3$ ) model was developed. This was also based on the volume of the weld and semi-infinite heat model. The temperatures were compared to the FEA as well as experimental measured temperatures.

## 3.4 Results and Discussion

### 3.4.1 Ultrasonic welding

Tables 3.2 and 3.3 describe the welding conditions for each sample and both tested amplitudes detailing the actual weld times associated with each weld velocity determined by iQ Explorer II to identify the primary control parameter of collapse ( $D$ ). The average weld time of the 3 repeated samples is detailed in the tables. As expected, it is seen that the weld time ( $t$ ) is generally proportional to collapse distance ( $D$ ) and generally inverse to weld velocity ( $V$ ). It is also seen that weld time is nearly independent of the amplitude. The weld time is actually dependent on the melt detect feature in the iQ Explorer II software. A higher amplitude will

generate energy more quickly, causing the melt detect feature to trigger at a lower weld time as is the case for the higher observed amplitude of  $32.4 \mu\text{m}_{p-p}$ .

Table 3.2. Design of experiments for  $21.6 \mu\text{m}_{p-p}$  amplitude.

D = 0.1 mm		D = 0.2 mm		D = 0.3 mm	
Velocity (mm/s)	Time (s)	Velocity (mm/s)	Time (s)	Velocity (mm/s)	Time (s)
0	0	0	0	0	0
1	0.152	1	0.248	1	0.331
0.8	0.173	0.8	0.284	0.8	0.410
0.6	0.228	0.6	0.344	0.6	0.516
0.4	0.283	0.4	0.517	0.4	0.707
0.2	0.504	0.2	0.918	0.2	1.395
0.1	0.926	0.1	1.779	0.1	2.678

Table 3.3. Design of experiments for  $32.4 \mu\text{m}_{p-p}$  amplitude.

D = 0.1 mm		D = 0.2 mm		D = 0.3 mm	
Velocity (mm/s)	Time (s)	Velocity (mm/s)	Time (s)	Velocity (mm/s)	Time (s)
0	0	0	0	0	0
1	0.107	1	0.194	1	0.289
0.8	0.126	0.8	0.233	0.8	0.351
0.6	0.163	0.6	0.309	0.6	0.456
0.4	0.233	0.4	0.445	0.4	0.700
0.2	0.452	0.2	0.919	0.2	1.290
0.1	0.899	0.1	1.732	0.1	2.650

Figures 3.17 to Figure 3.20 show the results from the tensile test performed for the ultrasonic welded samples at various weld distances and weld velocities. Samples were welded at a  $21.6 \mu\text{m}_{p-p}$  and  $32.4 \mu\text{m}_{p-p}$  amplitude, with each dot representing an average value for 3 repetitions and the error bars corresponding to one standard deviation ( $\pm 1$ ).

As seen in Figure 3.17 and 3.19, the ultimate stress was generally proportional to weld distance. This is probably the result of increased weld area, as the energy director melts, its

cross sectional area increases. In addition, as the weld velocities decreased for any given weld distance, there was higher heat diffusion in to the part and reduced shear thinning in the weld zone, which resulted in stronger welds. As seen in Figure 3.18 and 3.20, the ultimate strength was generally inversely proportional to melt velocity. This is consistent with other work that found that excessive melt velocity promotes poor molecular alignment because of shear thinning [8].

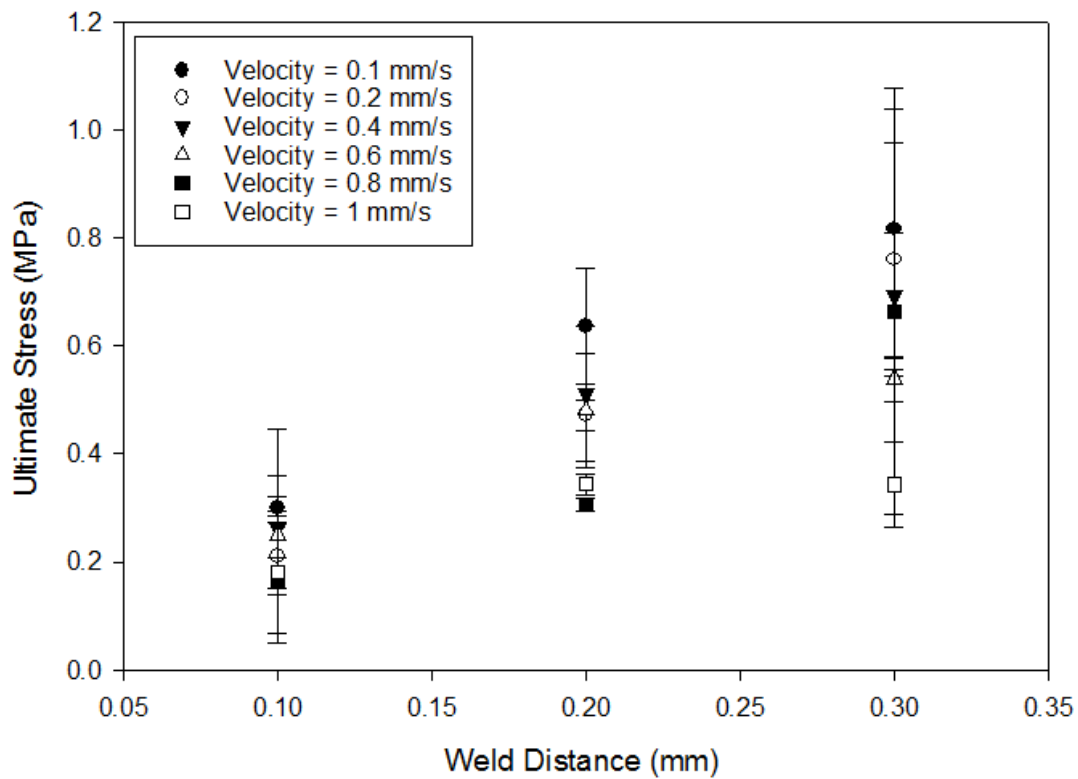


Figure 3.17. Ultimate Stress as a function of collapse distance at  $21.6 \mu\text{m}_{\text{p-p}}$  amplitude.

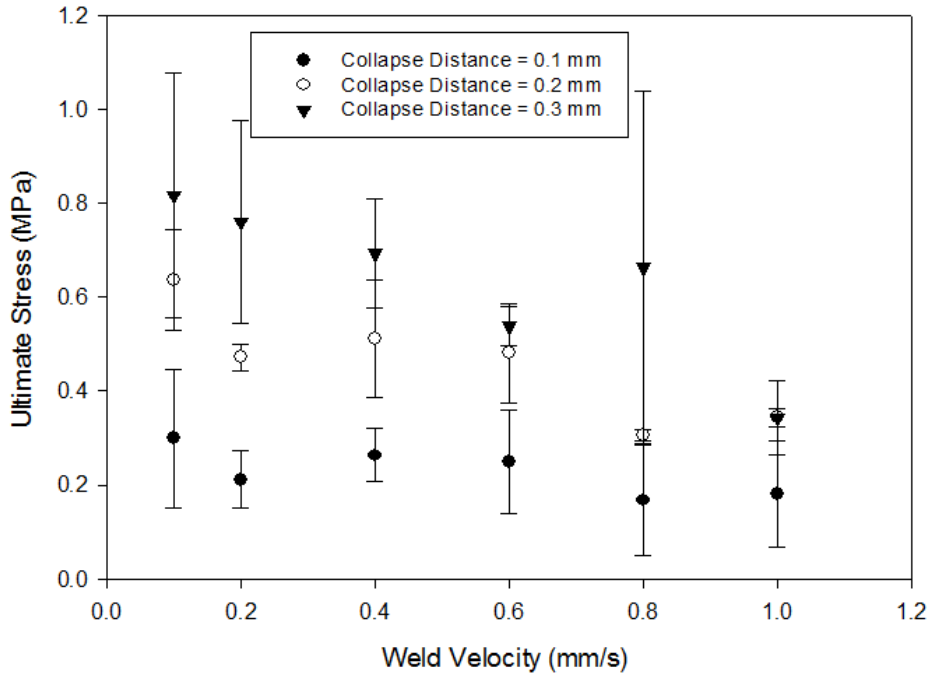


Figure 3.18. Ultimate Stress as a function of weld velocity at  $21.6 \mu\text{m}$  p-p amplitude.

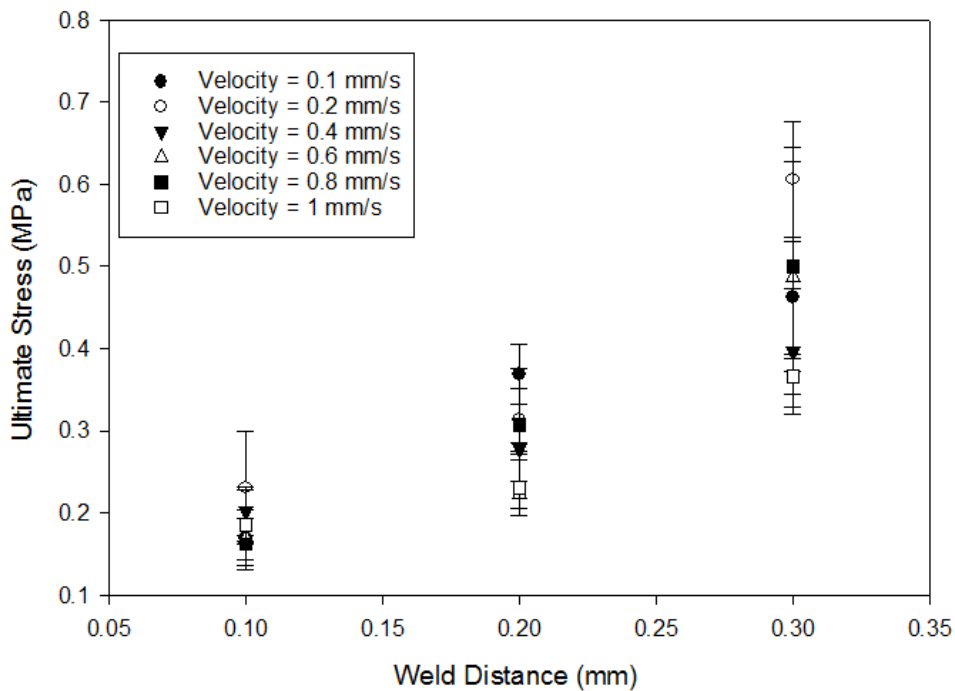


Figure 3.19. Ultimate Stress as a function of collapse distance at  $32.4 \mu\text{m}$  p-p amplitude.

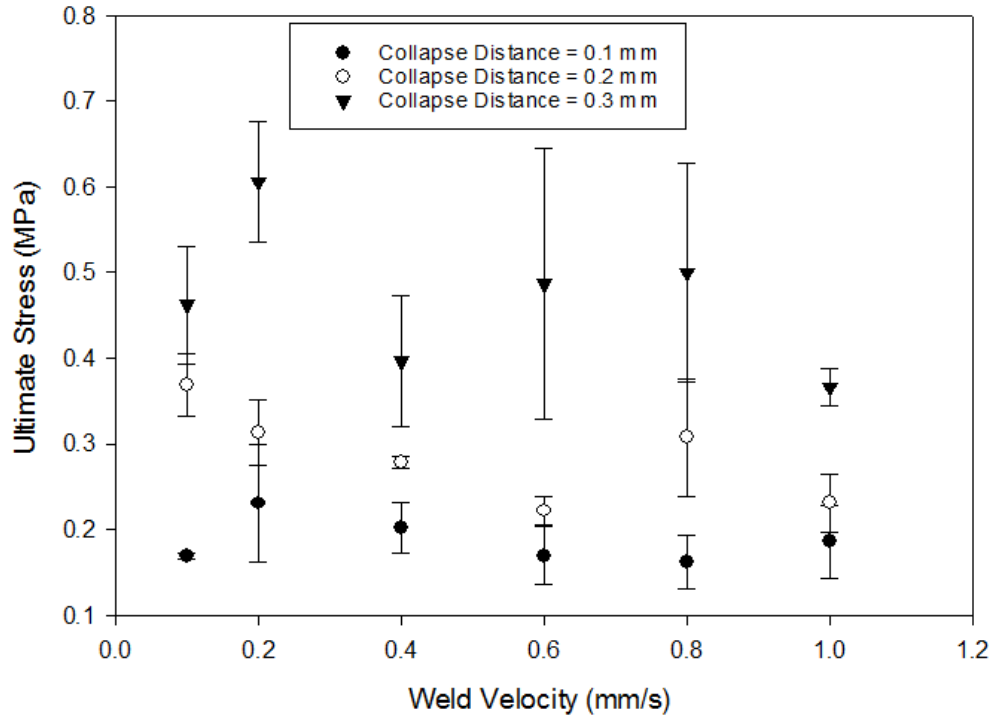


Figure 3.20. Ultimate Stress as a function of weld velocity at  $32.4 \mu\text{m}_{\text{p-p}}$  amplitude.

### 3.4.2 Ultrasonic modeling

The average machine power was used to calculate heat flux ( $\text{W}/\text{m}^2$ ) in order to predict temperature fields. The heat flux was used as a boundary condition (load) in an FEA ANSYS model. For comparison reasons, Figure 3.21 shows a Mathcad excerpt with model constants such as thermal conductivity, specific heat, and others used to calculate power. This power was compared to the power obtained through the ultrasonic welding machine for validation of the general heating model for ultrasonic welding [10]. In general, the two values were in good agreement. In Table 3.4, the theoretical power is compared to the measured machine power (the highest welding conditions) for both  $21.6 \mu\text{m}_{\text{p-p}}$  and  $32.4 \mu\text{m}_{\text{p-p}}$  amplitudes.

Table 3.4. Model theoretical power compared to measured machine power for both studied amplitudes.

Amplitude ( $\mu\text{m}_{\text{p-p}}$ )	Theoretical Power (W)	Machine Power (W)
21.6	137	160
32.4	308	248

It is important to note that because of the difficulty of measuring the loss modulus ( $E''$ ) at 20 kHz and elevated temperature, a value measured for polystyrene was used as a first order approximation [10].

Material properties:

$$\rho := 1189 \frac{\text{kg}}{\text{m}^3}$$

$$C := 1500 \frac{\text{J}}{\text{kg}\cdot\text{K}}$$

$$\lambda := .17 \frac{\text{W}}{\text{m}\cdot\text{K}}$$

$$E_{\text{loss}} := 0.18 \cdot 10^9 \text{ Pa}$$

$$f := 20000 \text{ Hz}$$

$$\omega := 2 \cdot \pi \cdot f \quad \omega = 1.257 \times 10^5 \frac{1}{\text{s}}$$

$$A_0 := (32.4 \cdot 10^{-6}) \text{ m}$$

$$\frac{A_{\text{loss}}}{A_0} := \frac{A_0}{2}$$

$$\frac{\varepsilon_{\text{loss}}}{\varepsilon} := \frac{A_0}{h} \quad \varepsilon = 0.065$$

Figure 3.21. Mathcad excerpt with material properties.

We proposed here to use a similar technique that allows researchers to estimate the loss modulus for a material at high frequencies and elevated temperatures. In more detail, by measuring bond line temperatures for a given amplitude and weld geometry, it is possible to

work backwards from the approach in Figure 3.21 to estimate the effective loss modulus. This novel proposed approach may be highly effective in determining the loss modulus for a range of materials. In Figure 3.22, the material properties detailed in Figure 3.21 were used to calculate volumetric heat rate ( $\text{W}/\text{m}^3$ ), which was then used to calculate power based on the initial volume of the energy director ( $\text{m}^3$ ).

Volumetric heating rates are based on the fundamental governing Equation 7 [6]:

$$\dot{Q} = \frac{E'' \omega \varepsilon_0^2}{2} \quad (7)$$

In this equation,  $E''$  is the material's effective loss modulus, which was estimated to be  $0.18 \times 10^9$  Pa as previously detailed. The angular frequency,  $\omega$ , is determined by the ultrasonic welding equipment which is 20 kHz, and  $\varepsilon$  is the mechanical strain based on amplitude/energy director height with a value of 0.043 when the amplitude condition tested was  $21.6 \mu\text{m}_{\text{p-p}}$ , and 0.065 when it is  $32.4 \mu\text{m}_{\text{p-p}}$ . As noted, the volumetric heating rate ( $\text{W}/\text{m}^3$ ) was used to determine the dissipated power based on the volume ( $\text{m}^3$ ) of the energy director to predict dissipated power (W). This dissipated power was 137 W for an amplitude of  $21.6 \mu\text{m}_{\text{p-p}}$  and 308 W for an amplitude of  $32.4 \mu\text{m}_{\text{p-p}}$ . The dissipated power obtained using the volumetric heating rate ( $\text{W}/\text{m}^3$ ) was compared to the average actual typical power from the ultrasonic welder ( $\sim 198$  W for  $21.6 \mu\text{m}_{\text{p-p}}$  and  $\sim 331$  W for  $32.4 \mu\text{m}_{\text{p-p}}$ ). The dissipated power was then used to determine the heat flux ( $\text{W}/\text{m}^2$ ) based on the faying surface area.



$$Q := \frac{E_{\text{loss}} \cdot \omega \cdot \epsilon^2}{2} \quad Q = 4.749 \times 10^{10} \cdot \frac{\text{W}}{\text{m}^3}$$

$$P := w \cdot h \cdot l \cdot Q$$

$$P = 308.21 \text{ W}$$

Figure 3.22. Mathcad excerpt finding power (P) from volumetric heat rate (Q).

When considering machine power to calculate transient thermal models, the power is divided by half because of the assumption of isothermal conditions in the z-direction for a semi-infinite body, in which case the energy flows in only one direction, while in the actual experiment it flow in two directions (upper and lower part). Table 3.5 details the actual average typical power from varying collapse distances and weld velocities for an amplitude of 21.6  $\mu\text{m}$  p-p. In Table 3.6, the same can be seen for an amplitude of 32.4  $\mu\text{m}$  p-p.

Table 3.5. Power (W) from ultrasonic welder at 21.6  $\mu\text{m}$  p-p amplitude.

Actual Power- Machine (W)		Collapse Distance (mm)		
		0.1	0.2	0.3
Weld Velocity (mm/s)	0.1	71	69	76
	0.2	70	76	89
	0.4	89	83	105
	0.6	106	95	142
	0.8	99	104	153
	1	98	102	160

Table 3.6. Power (W) from ultrasonic welder at 32.4  $\mu\text{m}$  p-p amplitude.

Actual Power- Machine (W)		Collapse Distance (mm)		
		0.1	0.2	0.3
Weld Velocity (mm/s)	0.1	142	129	134
	0.2	146	143	146
	0.4	148	153	161
	0.6	172	167	178
	0.8	149	190	210
	1	162	211	248

In Figure 3.23, the heat flux is calculated from the corresponding machine power for each welding condition. The heat flux values were used as input in ANSYS in order to obtain the predicted temperature profiles.

$$P := 283.17 \text{ W}$$

$$w_{fay} = 3 \cdot \text{mm}$$

$$l = 110 \cdot \text{mm}$$

$$q := \frac{P}{w_{fay} \cdot l} = 8.581 \times 10^5 \cdot \frac{\text{W}}{\text{m}^2}$$

Figure 3.23. Mathcad excerpt finding heat flux ( $q$ ) from actual machine power ( $P$ ).

Detailed in Tables 3.7 and 3.8 are the average heat flux values obtained from applying the heat flux formula in Figure 3.23.

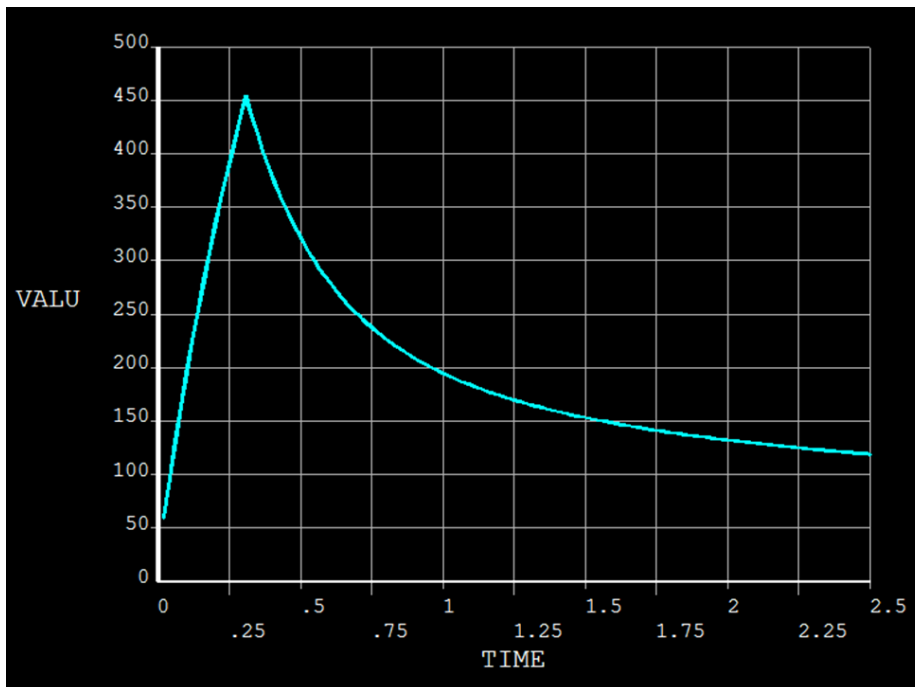
Table 3.7. Average heat flux ( $q$ ) for  $21.6 \mu\text{m}_{p-p}$ .

Heat flux ( $\text{W}/\text{m}^2$ )		Collapse Distance (mm)		
		0.1	0.2	0.3
Weld Velocity (mm/s)	0.1	2.1E+05	2.1E+05	2.3E+05
	0.2	2.1E+05	2.3E+05	2.7E+05
	0.4	2.7E+05	2.5E+05	3.2E+05
	0.6	3.2E+05	2.9E+05	4.3E+05
	0.8	3.0E+05	3.2E+05	4.6E+05
	1	3.0E+05	3.1E+05	4.8E+05

Table 3.8. Average heat flux ( $q$ ) for  $32.4 \mu\text{m}$  p-p.

Heat flux ( $\text{W}/\text{m}^2$ )		Collapse Distance (mm)		
		0.1	0.2	0.3
Weld Velocity (mm/s)	0.1	4.3E+05	3.9E+05	4.1E+05
	0.2	4.4E+05	4.3E+05	4.4E+05
	0.4	4.5E+05	4.6E+05	4.9E+05
	0.6	5.2E+05	5.1E+05	5.4E+05
	0.8	4.5E+05	5.8E+05	6.4E+05
	1	4.9E+05	6.4E+05	7.5E+05

A typical temperature profile based on the volumetric heating rate, established in Equation 7, that uses the strain and effective loss modulus stated previously is shown in Figure 3.24. This temperature profile is for a weld time of 0.321 seconds and machine power of 159. W. It is seen that relatively high temperatures are predicted. Note that these predicted temperature histories are similar to those experimentally measured with a type-K thermocouple, under the same welding conditions of weld time and machine power, as seen in Figure 3.25.

Figure 3.24. ANSYS Temperature profile ( $^{\circ}\text{C}$  as a function of time).

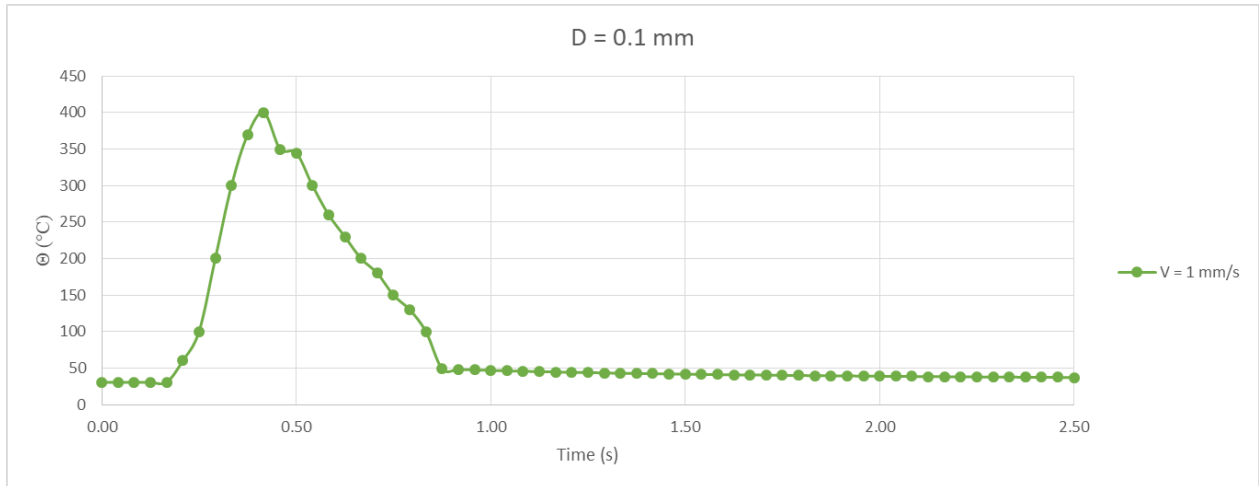


Figure 3.25. Type-K thermocouple 36-gauge temperature profile.

The ANSYS temperature profiles for all samples at varying weld distances and weld velocities were imported into Excel, where each individual degree of weld were calculated and later summed to obtain the total degree of weld.

A sample degree of weld calculation template is shown in Figure 3.26 for sample A3 (0.4 mm/s weld velocity, 0.1 mm weld distance and  $21.6 \mu\text{m}_{p-p}$  amplitude).

Time	$\Delta t$	$\Theta$ -Celsius	$\Theta$ -Kelvin	$K_0$	$E_a$	R	DW	DW total
1.74	0.02	168.42	441	9.66	2.86E+04	8.314	0.0015083	0.599381666
1.76	0.02	167.28	440	9.66	2.86E+04	8.314	0.0014781	0.600859795
1.78	0.02	166.16	439	9.66	2.86E+04	8.314	0.0014491	0.602308913
1.80	0.02	165.07	438	9.66	2.86E+04	8.314	0.0014212	0.603730132
1.82	0.02	164.01	437	9.66	2.86E+04	8.314	0.0013944	0.605124483
1.84	0.02	162.97	436	9.66	2.86E+04	8.314	0.0013685	0.606492964
1.86	0.02	161.96	435	9.66	2.86E+04	8.314	0.0013435	0.607836497
1.88	0.02	160.97	434	9.66	2.86E+04	8.314	0.0013195	0.609155977
1.90	0.02	160.00	433	9.66	2.86E+04	8.314	0.0012962	0.610452226
1.92	0.02	159.05	432	9.66	2.86E+04	8.314	0.0012738	0.611726068

↓

1.88	0.02	160.97	434	9.66	2.86E+04	8.314	=E96*(EXP(-F96/(G96*D96)))*B96^(1/4))
------	------	--------	-----	------	----------	-------	---------------------------------------

Figure 3.26. Excel excerpt of degree of weld calculation for 0.4 mm/s weld velocity, 0.1 mm weld distance and  $21.6 \mu\text{m}_{p-p}$  amplitude (Sample A3).

This highlighted total degree of weld (DW total) was then multiplied by the highest ultimate stress for each collapse distance within both studied amplitudes to yield final predicted strengths.

### 3.4.3 Model validation

In order to verify the accuracy of the predicted data, the actual measured strengths were compared to the final predicted strengths in the models. Initially graphs plotting weld strength as a function of weld time are considered. The weld time is dependent on the weld velocities. A weld time was determined from the iQ Explorer II software. This means there is a total of six different weld times (average) for the six studied weld velocities as indicated on Tables 3.2 and 3.3 of this discussion. In Figure 3.27, the welding parameters were amplitude and collapse distance at  $21.6 \mu\text{m}_{p-p}$  and 0.1 mm, respectively. It can be seen that the model and experimental data are generally well aligned. Figure 3.28 shows the data for  $21.6 \mu\text{m}_{p-p}$  amplitude and 0.2 mm of collapse distance. Again, it is seen that the model predicts the weld strength reasonably well, with complete healing being achieved under the last two welding condition.

Figure 3.29 shows data for an amplitude of  $21.6 \mu\text{m}_{p-p}$  and a collapse distance of 0.3 mm. In this plot, complete healing is achieved earlier than under the conditions displayed in Figures 3.27 and 3.28. This is can likely be attributed to better welding conditions at higher collapse distance (0.3 mm). The model is again in agreement with the experimental data.

Figure 3.30 shows the actual weld strength as a function of predicted weld strength for collapse distances 0.1 mm, 0.2 mm and 0.3 mm for an amplitude of  $21.6 \mu\text{m}_{p-p}$ . The plot shows good agreement between the predicted and actual weld strength, with an R squared of 0.78.

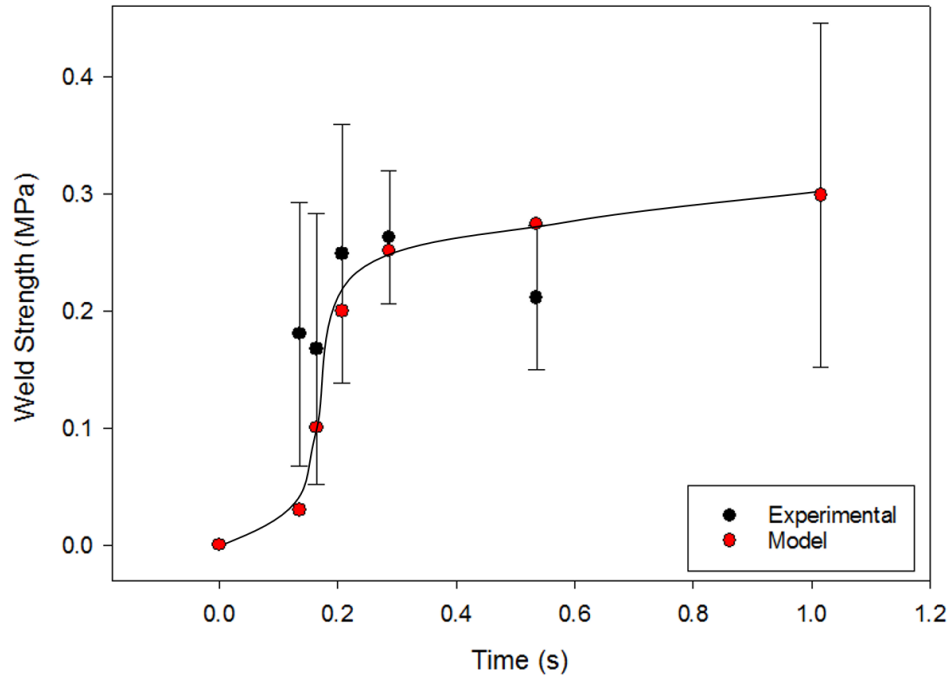


Figure 3.27. Model validation at  $21.6 \mu\text{m}$   $p\text{-}p$  amplitude and 0.1 mm collapse distance.

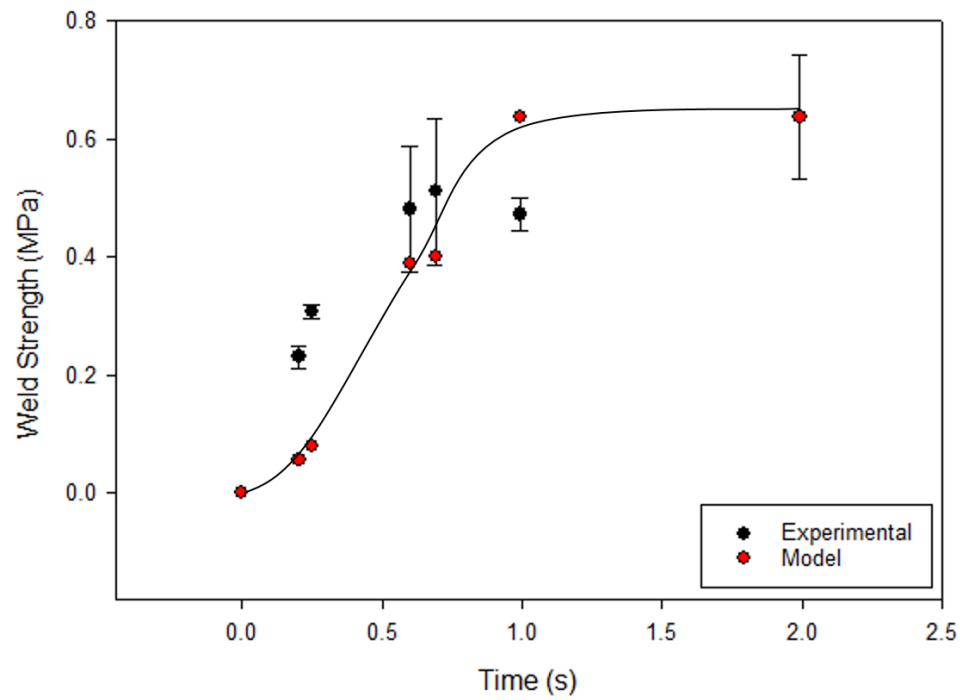


Figure 3.28. Model validation at  $21.6 \mu\text{m}$   $p\text{-}p$  amplitude and 0.2 mm collapse distance.

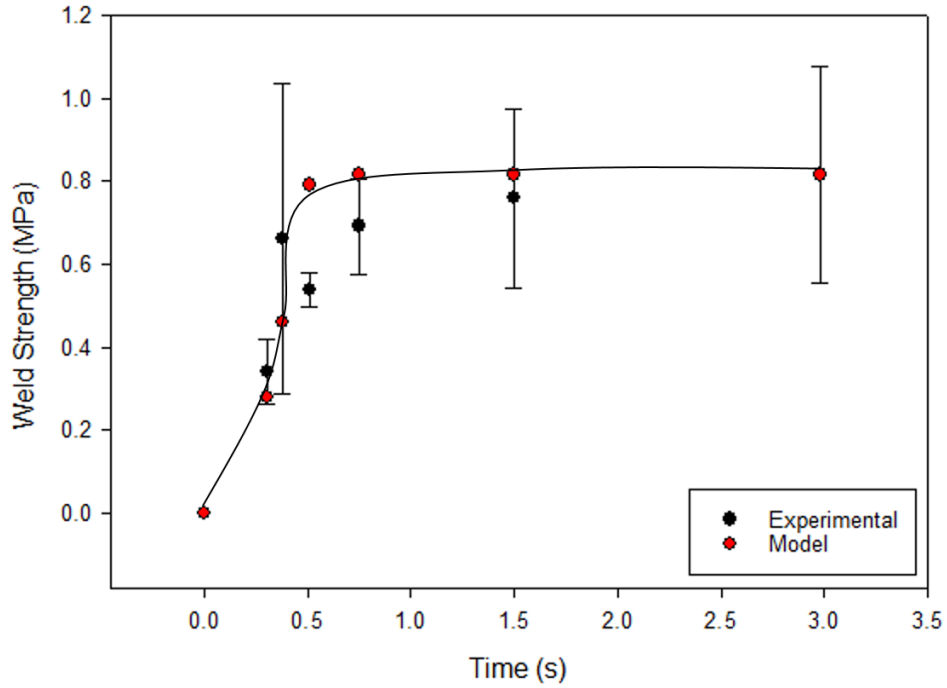


Figure 3.29. Model validation at  $21.6 \mu\text{m}$   $p\text{-}p$  amplitude and 0.3 mm collapse distance.

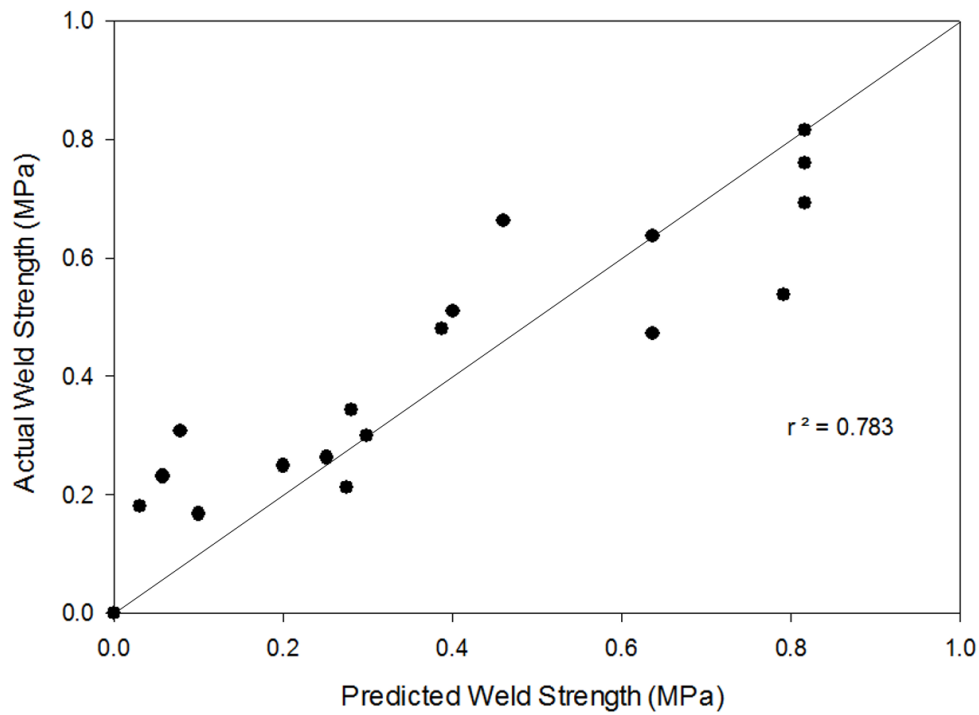


Figure 3.30. Collapsed data of actual weld strength as a function of predicted weld strength at  $21.6 \mu\text{m}$   $p\text{-}p$  amplitude.

In Figure 3.31, the amplitude was  $32.4 \mu\text{m}_{\text{p-p}}$  and the collapse distance was  $0.1 \text{ mm}$ , respectively. Both the model and the experimental data are in good agreement. The amplitude in Figure 3.32 was  $32.4 \mu\text{m}_{\text{p-p}}$  and the collapse distance was  $0.2 \text{ mm}$ . It is seen that the weld strength is generally proportional to time with an inflection point at 1 second. Again, the model is in reasonable agreement with the experimental data. In Figure 3.33, the amplitude was  $32.4 \mu\text{m}_{\text{p-p}}$  with a collapse distance of  $0.3 \text{ mm}$ , and it is seen that in general, the models predict the weld strength with good agreement. It was observed that in Figures 3.31, 3.32 and 3.33 ( $32.4 \mu\text{m}_{\text{p-p}}$  amplitude), weld strengths were slightly lower than in Figures 3.27, 3.28 and 3.29, which represented a lower amplitude of  $21.6 \mu\text{m}_{\text{p-p}}$ . A possible explanation could be the fact that some samples under the higher amplitude experienced over-welding, which resulted in poor molecular alignment and shear thinning. Figure 3.34 shows the collapsed data for  $32.4 \mu\text{m}_{\text{p-p}}$  amplitude where the weld strength is plotted as a function of predicted weld strength for all the data. The R squared value for all the compiled data was determined as well with an R squared of 0.77.

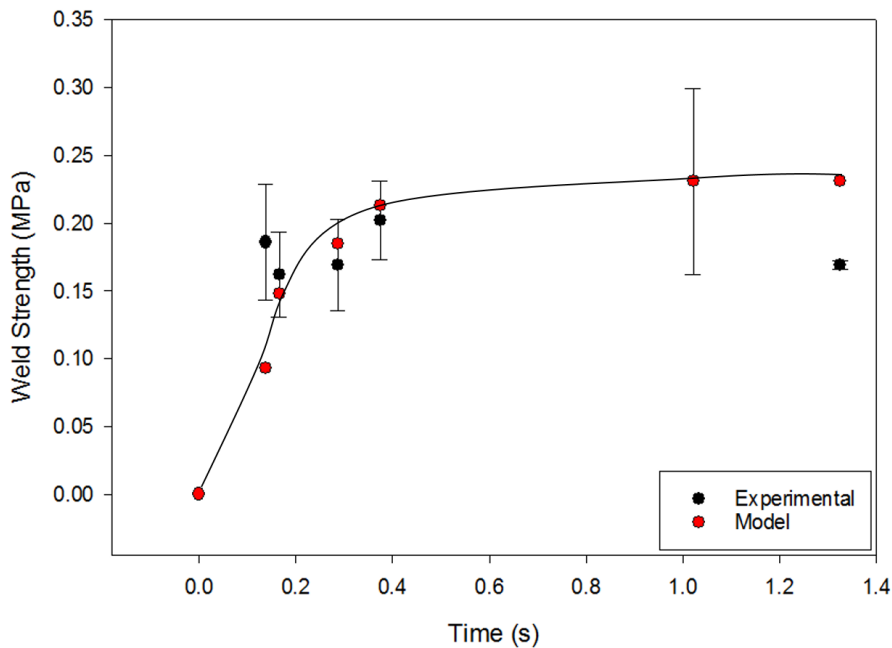


Figure 3.31. Model validation at  $32.4 \mu\text{m}_{\text{p-p}}$  amplitude and  $0.1 \text{ mm}$  collapse distance.



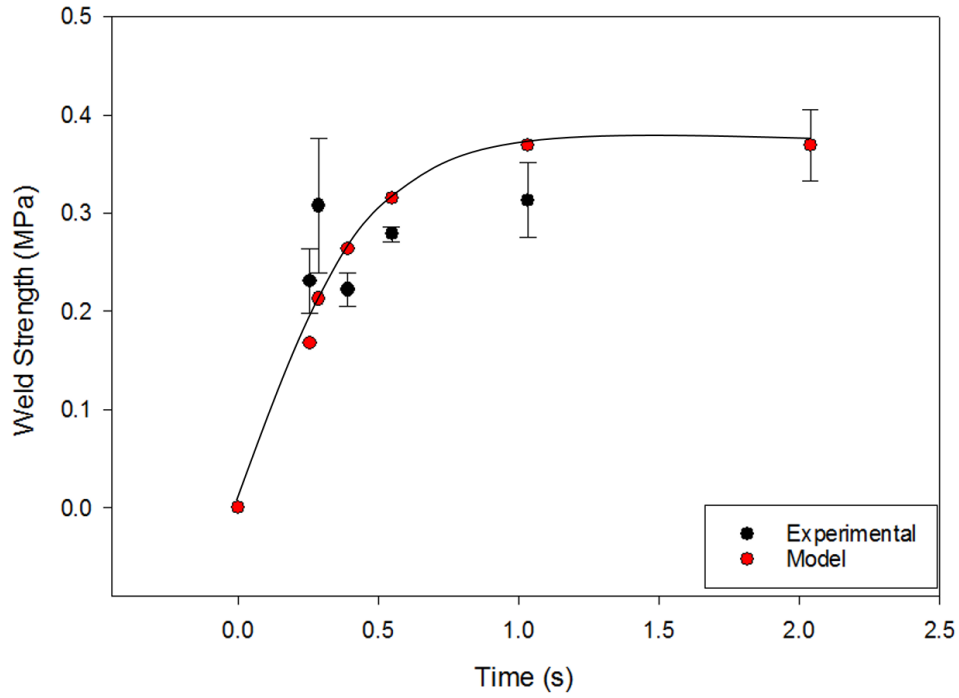


Figure 3.32. Model validation at  $32.4 \mu\text{m}$   $p\text{-}p$  amplitude and 0.2 mm collapse distance.

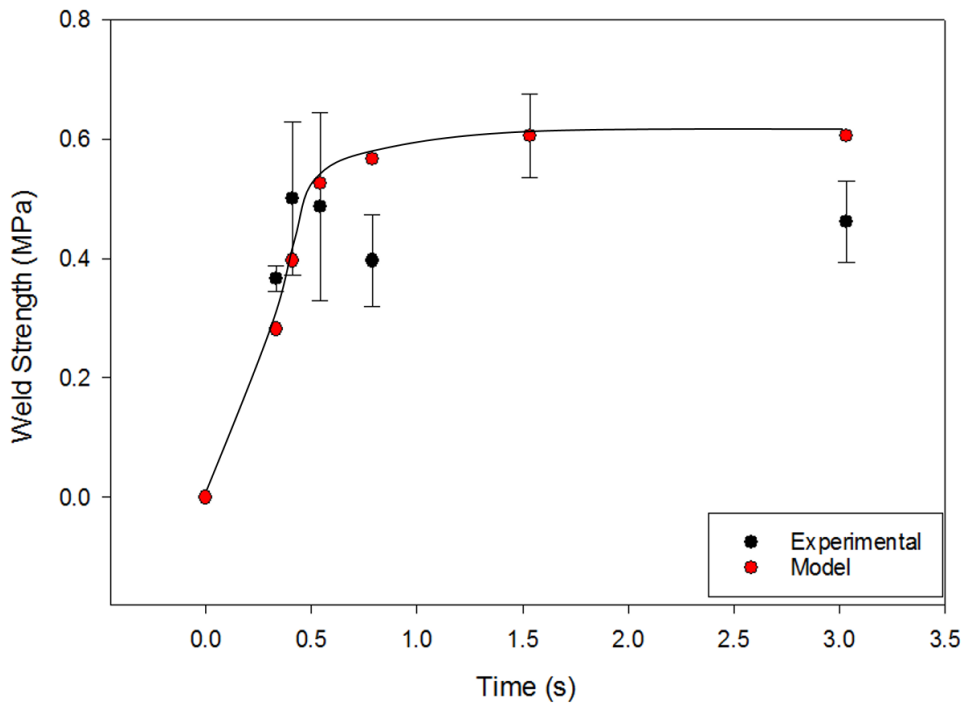


Figure 3.33. Model validation at  $32.4 \mu\text{m}$   $p\text{-}p$  amplitude and 0.3 mm collapse distance.

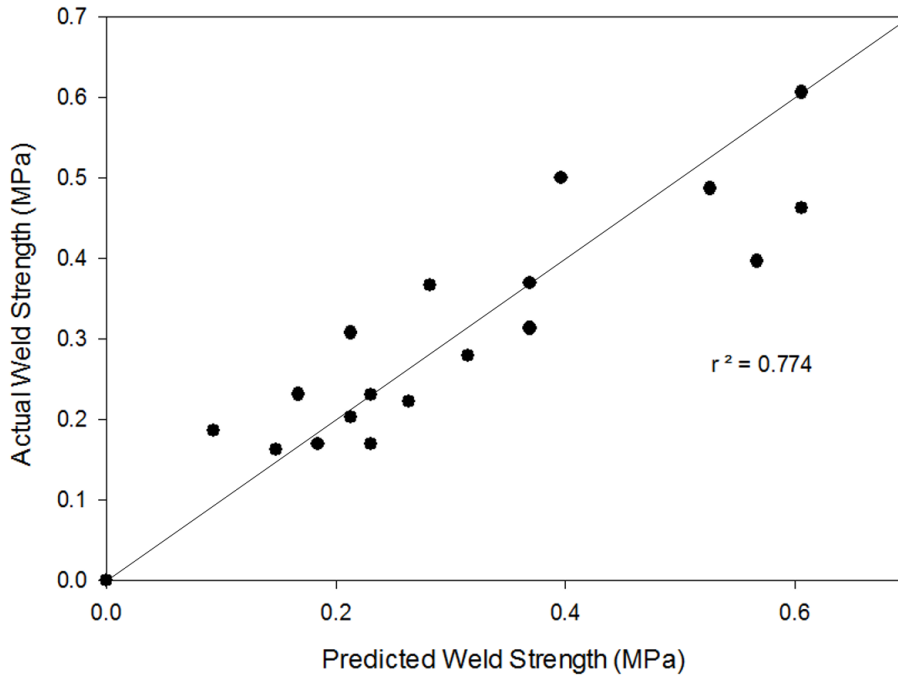


Figure 3.34. Collapsed data of actual weld strength as a function of predicted weld strength at  $32.4 \mu\text{m}_{\text{p-p}}$  amplitude.

### 3.5 Conclusion

This study validated experimental data with models based on molecular healing and activation energy. The modeling from ANSYS, coupled with activation energy, was able to be used to predict weld strength. By plotting the collapsed data, it was possible to find that there was an R squared value of 0.78 between the actual weld strength and the predicted weld strength for an amplitude of  $21.6 \mu\text{m}_{\text{p-p}}$ , and an R squared value of 0.77 between the actual weld strength and the predicted weld strength for an amplitude of  $32.4 \mu\text{m}_{\text{p-p}}$ .

### 3.6 References

1. Grewell, D. Modeling of molecular healing for micro-laser welding of plastics with diffractive optical elements as spatial modulators. Electronic Thesis or Dissertation. Retrieved from <https://etd.ohiolink.edu/>. 2005.
2. Vogel, J. Sealing and cutting of PLA bio-plastic. Graduate Theses and Dissertations. 14131. <http://lib.dr.iastate.edu/etd/14131>. 2011.
3. Grewell, D. Welding of Plastics: Fundamentals and New Developments. Intern. Polymer Processing, 1, 43-60. 2007.
4. The Welding Institute. Ultrasonic welding of injection molded components. Retrieved June 19, 2016, from <http://www.twi-global.com/technical-knowledge/job-knowledge/ultrasonic-welding-of-injection-moulded-components-part-1-process-and-equipment-061/>. 2016.
5. Wool, R. Polymer interfaces: structure and strength. Hanser Publishers; Cincinnati: Distributed in the USA and in Canada by Hanser/Gardner Publications, Munich; New York. 1994.
6. Loos, A.C., Dara P.H. Thermoplastic Matrix Composites Processing Model, Interim Report 57, NASE Cooperative Agreement NAG-1-343. 1985.
7. De Gennes, P.G. Reptation of a Polymer Chain in the Presence of Fixed Obstacles. Journal of Chemical Physics, 55, 572. 1971.
8. Grewell, D., Benatar, A. Semiempirical, squeeze flow, and intermolecular diffusion model. II. Model verification using laser microwelding. (Technical report). Polymer Engineering and Science, 48(8), 1542-1549. 2008.
9. Marcus, E. M., Golko, P., Lester, S., Klinstein, L. Comparison of Servo-Driven Ultrasonic Welder to Standard Pneumatic Ultrasonic Welder. ANTEC 2009.
10. Benatar, A., Gutowski, T. Ultrasonic welding of PEEK graphite APC-2 composites. Polymer Engineering and Science, 29(23), 1705-1721. 1989.

**CHAPTER 4****GENERAL CONCLUSIONS**

This study showed that it was possible to use molecular healing models based on an activation energy calculation to predict weld strength. Furthermore, this work demonstrated that while the weld process is complex and considers thermal transfer, molecular diffusion and squeeze flow, these models can be coupled into one model that accurately predicts the level (degree) of welding. In addition, it was shown that activation energy can be used to predict weld strength.